1   Some mechanistic underpinnings of molecular adaptations of SARS-COV-2 spike

2   protein by integrating candidate adaptive polymorphisms with protein dynamics

3   Nicholas J. Ose[1], Paul Campitelli[1], Tushar Modi[1], I. Can Kazan[1], Sudhir Kumar[2,3,4,*] and S. Banu Ozkan[1,*]

4

5

6   [1]Department of Physics and Center for Biological Physics, Arizona State University, Tempe, Arizona,

7   United States of America

8   [2]Institute for Genomics and Evolutionary Medicine, Temple University, Philadelphia, Pennsylvania,

9   United States of America

10   [3]Department of Biology, Temple University, Philadelphia, Pennsylvania, United States of America

11   [4]Center for Genomic Medicine Research, King Abdulaziz University, Jeddah, Saudi Arabia

12

13

14

15   * s.kumar@temple.edu (SK); * Banu.Ozkan@asu.edu (SBO)

16

17

18   **Abstract**

19   We integrate evolutionary predictions based on the neutral theory of molecular evolution with protein

20   dynamics to generate mechanistic insight into the molecular adaptations of the SARS-COV-2 Spike (S)

21   protein. With this approach, we first identified Candidate Adaptive Polymorphisms (CAPs) of the SARS-

22   CoV-2 Spike protein and assessed the impact of these CAPs through dynamics analysis. Not only have we

23   found that CAPs frequently overlap with well-known functional sites, but also, using several different

24   dynamics-based metrics, we reveal the critical allosteric interplay between SARS-CoV-2 CAPs and the S

25   protein binding sites with the human ACE2 (hACE2) protein. CAPs interact far differently with the hACE2

26   binding site residues in the open conformation of S protein compared to the closed form. In particular,

27   the CAP sites control the dynamics binding residues in the open state, suggesting an allosteric control of

28   hACE2 binding. We also explored the characteristic mutations of different SARS-CoV-2 strains to find

29   dynamic hallmarks and potential effects of future mutations. Our analyses reveal that Delta strain-specific

30   variants have non-additive (i.e., epistatic) interactions with CAP sites, whereas the less pathogenic

31   Omicron strains have mostly compensatory variants. Finally, our dynamics-based analysis suggests that

32   the novel mutations observed in the Omicron strain epistatically interact with the CAP sites to help escape

33   antibody binding.

34   **Introduction**

35   Since 2019, the evolution of SARS-CoV-2 in humans has been characterized by the spread of mutations,

36   many notably found within the Spike (S) glycoprotein. The S protein is directly related to the human

37   immune response to COVID-19 and, as such, has been one of the most studied and targeted proteins in

38   the SARS-CoV-2 research (Shang et al. 2020; Harvey, Carabelli, Jackson, Gupta, Thomson, Harrison,

39   Ludden, Reeve, Rambaut, Consortium, et al. 2021; Jackson et al. 2022; Carabelli et al. 2023; Markov et al.

40   2023). Subsequently, research into the biophysical properties and mutational patterns associated with S

41   protein evolution not only remains critical to understanding the pandemic but also emerges as a useful

42   system to understand the mechanics of molecular adaptation within viruses.

43   For successful infection of a human host, the S glycoprotein of SARS-CoV-2 binds to the human ACE2

44   (hACE2) receptor through its receptor-binding domain (RBD). Evidence indicates that fine-tuning S protein

45   interactions with hACE2 significantly affects viral reproduction (Rehman et al. 2020; Saputri et al. 2020;

46   Rochman et al. 2021). Previous evolutionary studies show a complex network of interactions among

47   mutated residues (Changeux and Edelstein 2005; Doshi et al. 2016; O'Rourke et al. 2016; Mishra and

48   Jernigan 2018). Therefore, there has been a vast effort to uncover which mutations are important steps

49   of adaptation for the S protein (Cagliani et al. 2020; Damas et al. 2020; Singh and Yi 2021; Kistler et al.

50   2022; Maher et al. 2022; Neher 2022). In particular, a significant aspect of many such studies was a focus

51   on understanding adaptive mutations of SARS-CoV-2 that contributed to the leap to human hosts (Cagliani

52   et al. 2020; Damas et al. 2020; Singh and Yi 2021; Starr, Zepeda, et al. 2022). This is because SARS-CoV-2

53   has continuously mutated since its early detection (Kistler et al. 2022), causing the emergence of CDC-

54   designated "variants of concern" (VOCs) that an accelerated substitution rate may drive (Tay et al. 2022).

55   Predicting how new mutations impact the biophysical properties of the S protein remains a challenge, let

56   alone explaining their complex interactions with one-another and how they might affect hACE2 binding

57   because many factors affect hACE2 interactions. Binding affinity with hACE2 can be enhanced directly

58   through stronger receptor interactions or mediated through changes in RBD opening (Teruel et al. 2021;

59   Zhang et al. 2021; Díaz-Salinas et al. 2022). The RBD exhibits both 'closed' and 'open' conformational

60   states. In the closed state, the RBD is shielded from receptor binding. In the open state, the RBD is

61   accessible for hACE2 binding (Kirchdoerfer et al. 2016; Gur et al. 2020; Henderson et al. 2020; Hoffmann

62   et al. 2020). While some mutations may affect the transition between these states (Henderson et al. 2020;

63   Yurkovetskiy et al. 2020; Gobeil, Janowska, McDowell, Mansouri, Parks, Manne, et al. 2021; Sztain et al.

64   2021; Zhang et al. 2021; Shoemark et al. 2022), the other mutations may allosterically regulate RBD

65   openings through Furin cleavage site (residue ID range: 681-695) interactions to regulate hACE2 binding

66   (Deng et al. 2021; Gobeil, Janowska, McDowell, Mansouri, Parks, Stalls, et al. 2021; Khan et al. 2021;

67   Laiton-Donato et al. 2021).

68   Moreover, as new mutations accumulate, culminating in the emergence of a new VOC, these mutations

69   must occur on varied sequence backgrounds containing neutral, nearly-neutral, and adaptive mutations.

70   While many studies have explored the impacts of individual mutations, VOCs result in a substantial

71   difference in protein function compared to their individual effects (Moulana et al. 2022a; Starr, Greaney,

72   Hannon, et al. 2022; Moulana et al. 2023; Witte et al. 2023). Here we integrate an evolutionary approach

73   with protein dynamics analysis to address the fundamental mechanisms of mutations dictating the VOCs

74   and the impact of their epistatic interaction on the function of the S protein. Many earlier studies have

75   combined phylogeny and evolutionary theory to identify adaptive mutations as well as to see how the

76   viral sequence has changed over time (Frost et al. 2018; Boni et al. 2020; Cagliani et al. 2020; Damas et al.

77   2020; Tang et al. 2020). Similarly, we first use a well-established Evolutionary Probability (EP) approach

78   (Liu et al. 2016) that utilizes phylogenetic trees in combination with the neutral theory of molecular

79   evolution to determine Candidate Adaptive Polymorphisms (CAPs) determined using the early Wuhan

80   sequence as a variant. CAPs are substitutions in SARS-CoV-2 that are rarely observed in other closely

81   related sequences (Figure 1A), which implies a degree of functional importance and makes them

82   candidates for adaptation (Liu et al. 2016). In support of this method, we find an overlap between our list

83   of sites containing CAPs and putative adaptive sites identified by others (Cagliani et al. 2020; Singh and Yi

84   2021; Starr, Zepeda, et al. 2022). Second, we use a suite of computational tools to analyze how CAPs that

85   arose in the early and late phases of the COVID-19 pandemic modulate the dynamics of the S protein. We

86   also explore the complex interactions between these sets of CAPs to gain mechanistic insight into the

87   behavior of molecular adaptation involving the S protein. In particular, we focused on how mutations

88   modulate protein dynamics, as we and others have previously found that rather than changing a protein's

89   structure solely, mutations modulate conformational dynamics leading to changes in biophysical

90   properties such as stability, flexibility, and allosteric dynamic coupling, any of which may affect protein

91   binding (Swint-Kruse et al. 1998; Keskin et al. 2000; Bhabha et al. 2013; Nussinov, R., Tsai, C.-J 2013;

92   Campbell, E. et al. 2016; Ma and Nussinov 2016: 201; Saavedra et al. 2018; Kuzmanic et al. 2020).

93   With this evolutionary-dynamics unified approach, we aim to answer the following questions about VOCs:

94   Are all the mutations in VOCs adaptive in nature? Are they coupled to one another or provide some

95   measure of biophysical, dynamical, or mechanical compensation? While many of these mutations are

96   found within the RBD domain, numerous others are located distal to this region; hence, we aim to

97   investigate the functional roles of distal mutations, particularly from a protein dynamics perspective. Our

98   integrated analysis revealed that protein dynamics play a significant role in the evolution of the S protein.

99   The flexibility of sites withing the S protein shows a strong, direct correlation with substitution rate, and

100   newly evolving CAPS are mostly compensatory (i.e., additive) mutations that modulate the dynamics of

101   the hACE2 binding site. Yet other CAPs, 346R, 486F, and 498Q, show highly epistatic (i.e., non-additive)

102   modulation of the hACE2 binding site and provide immune escape benefits.

103

104   **Results and Discussions**

105   **Candidate Adaptive mutations in the Spike protein are recognized via Evolutionary Probabilities.**

106   SARS-CoV-2 is part of a family of coronaviruses, many of which infect mainly animals and are less capable

107   of infecting humans (Dicken et al. 2021). Therefore, to identify the most likely mutations responsible for

108   the infection of human hosts (i.e., putative adaptive mutations for humans), we estimated the (neutral)

109   evolutionary probability (EP) scores of mutations found within the S protein (Liu et al. 2016). EP scores of

110   the amino acid variants of S protein are obtained by constructing a maximum likelihood phylogenetic tree

111   (Goldman 1990) containing 19 orthologous coronavirus sequences, which were selected based on the

112   amount of divergence over evolutionary history to ensure that each amino acid position had ample time

113   to experience purifying selection (Patel et al. 2018) (Figure 1A). The likelihood of finding a particular amino

114   acid in the sequence is then determined using a Bayesian framework, with calculations carried out by

115   MEGA X software (Kumar et al. 2018). As apparent in the name, EP scores obtained for the amino acids in

116   the sequence provide information regarding the likelihood of finding them at their position, given the

117   history of the sequence. Amino acid residues receiving low EP scores (<0.05) at a position are less likely to

118   be found in a given position within the sequence because they are non-neutral. Generally, positions with

119   low EP amino acids are far less common than those containing mutations with high EP, a trend also

120   realized in the CoV-2 S protein (Figure 1B).

121   Of particular interest is an observed evolutionary change where an amino acid with high EP is replaced by

122   an amino acid residue with low EP. While amino acids with low EP should be harmful or deleterious to

123   viral fitness due to functional disruption or change, fixation of a low EP amino acid at a position suggests

124   an underlying mechanism for natural selection to operate. These fixed, low EP mutations are called

125   candidate adaptive polymorphisms (CAPs) as they are predicted to alter protein function, and adaptive

126   pressures may drive their prevalence (Patel et al. 2018). Indeed, there is an overlap between these CAPs

127   and the mutations suggested by other methods to be adaptive for the S protein (Cagliani et al. 2020; Singh
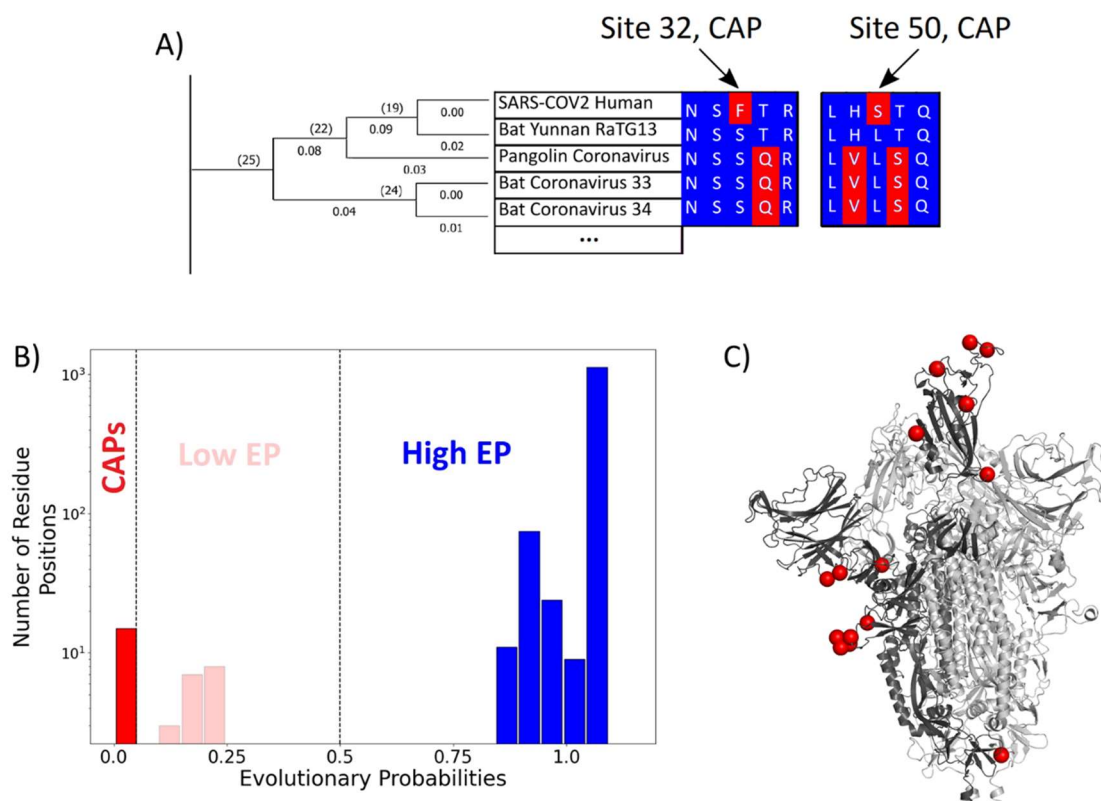
128   and Yi 2021; Starr, Zepeda, et al. 2022).

Figure 1. (A) The evolutionary probabilities (EP) of each amino acid in the S protein sequence are calculated by taking the multiple sequence alignment of the S proteins through their evolutionary tree and using Bayesian inferences to determine the likelihood of finding a particular residue at a particular location within a given sequence. Simply, if the residue is found at a location 'x' in closely related sequences, it will have a higher EP at location 'x' in the target sequence. Residues with an EP <0.05 in the target sequence are CAPs (Red). (B) The distribution of EP scores of the wild-type residues in the S protein. Here, lower EP scores are shown in red, and higher EP scores in blue. While the vast majority of the wild-type (reference) protein consists of high EP residues, a few residues have low EP. (C) The CAPs are also highlighted as red spheres in the open configuration of the S protein, with the open chain in a darker shade. We observe that a majority of the CAP positions reside at the receptor binding domain (RBD) and the Furin cleavage site (676-689; (Wrobel et al. 2020)) shown as transparent light gray spheres.

Interestingly, most of the CAP residues are in functionally critical sites, including the receptor binding domain (RBD) and the Furin cleavage site (Figure 1C). As mentioned earlier, the RBD plays a key role in initiating the infection of a healthy cell by binding it with the host organism's ACE2 protein. Before ACE2

144   binding, one chain of the homotrimer comprising the S protein must open to expose the RBD (Kirchdoerfer

145   et al. 2016; Henderson et al. 2020; Hoffmann et al. 2020; Sztain et al. 2021). The Furin cleavage site plays

146   a key role in the opening process as it aids in the cleavage of the S protein into two domains: S1 and S2

147   (Wrobel et al. 2020: 13). Similar cleavage sites have been found in related coronaviruses, including HKU1

148   and Middle East respiratory syndrome coronavirus (MERS-CoV), which infect humans (Chan et al. 2008:

149   1; Millet and Whittaker 2014; Millet and Whittaker 2015), and the acquisition of similar cleavage sites is

150   associated with increased pathogenicity in other viruses such as the influenza virus (Steinhauer 1999).

151   Interestingly, however, CAPs do not display such an overwhelming tendency to occur at well-known

152   critical sites within human proteins studied with similar methods (Ose, Campitelli, et al. 2022), yet

153   mutations at those sites are associated with disease, indicating their critical role in inducing functional

154   change. Therefore, the identified CAPs in the S protein, which are signs of recent evolution, can provide

155   mechanistic insights regarding the molecular adaptation of the virus. In particular, we aimed to analyze

156   how these CAP positions in the S protein modulate the interaction with hACE2 using our protein dynamics-

157   based analysis (Gerek and Ozkan 2011; Nevin Gerek, Z., Kumar, S., Banu Ozkan, S. 2013; Larrimore et al.

158   2017; Kumar, A., Glembo, T.J., Ozkan, S.B. 2015b).

159

160   **Asymmetry in communications among the network of interactions in Spike describes how CAPs regulate**

161   **the dynamics of the Spike protein.**

162   A mutation at a given amino acid position inevitably not only alters local interactions, but this change

163   cascades through the residue-residue interaction network, which gives rise to a variation in native

164   ensemble dynamics to modulate function (Dror et al. 2012; Labbadia and Morimoto 2015; Sekhar and Kay

165   2019; Campitelli et al.). Thus, we analyze the internal dynamics of the system to understand the functional

166   role of CAPs in S proteins. This analysis allows us to gain a mechanistic understanding of the relationship

167   between CAP mutations and biophysical outcomes (Teruel et al. 2021). First, we implement the Dynamic

168   Coupling Index (DCI) approach to study long-distance coupling between the CAPs and the hACE2 binding

169   sites emerging from the 3D network of interactions across the S protein system. The DCI parameter

170   combines Perturbation Response Scanning and Linear Response Theory to capture the strength of a

171   displacement response for position *i* upon perturbation of position *j*, relative to the average fluctuation

172   response of position *i* to all other positions in the protein. It represents the strength of dynamic coupling

173   between positions *i* and *j* upon perturbation to *j.*

174   Further, asymmetry can be captured in the DCI values, as dynamic coupling is not necessarily due to an

175   anisotropic network. That is, each amino acid has a set of positions to which it is highly coupled, and this

176   anisotropy in connections gives rise to unique differences in coupling between a given *i, j* pair of amino

177   acids which do not have direct interactions. By calculating the coupling of the hACE2 binding interface in

178   the RBD with respect to the CAP residue positions and vice versa, we can generate DCI_{asym} (Figure 2A) as

179   the difference between the normalized displacement response of position *j* upon a perturbation to

180   position *i* (DCI_{ij}) and the normalized displacement response of position *i* upon a perturbation to position *j*

181   (DCI_{ji}) (See Methods). If the DCI_{asym} values significantly differ from zero, it shows asymmetry in coupling

182   and presents a cause-effect relationship between the *i, j* pair in terms of force/signal propagation. This

183   metric has been used previously in a variety of systems to analyze the unique behavior of positions within

184   a protein and a given position's propensity to effect biophysical changes upon mutation, particularly at

185   long distances (Modi and Ozkan 2018; Campitelli and Ozkan 2020; Kolbaba-Kartchner et al. 2021; Ose,

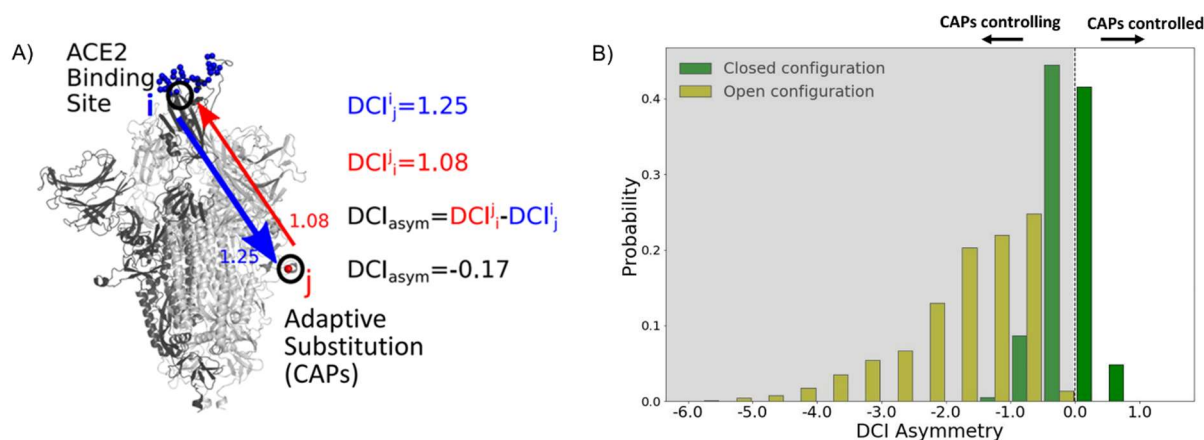186   Butler, et al. 2022; Kazan et al. 2023; Campitelli et al. 2020b).

187

Figure 2. (A) Schematic representation of DCI asymmetry. (B) DCI asymmetry of CAP residue positions with the binding interface of RBD in the open chain. Residues in the closed chains with a low EP amino acid in the reference sequence dominate the binding site interface of RBD in the open chain. There is a significant difference between the asymmetry profiles of the closed (M = -0.06, SD = 0.33) and open (M = -1.68, SD = 0.89) conformations (p < .001).

Recent work from our group has shown an enhancement in cross-chain communication within the main protease of SARS COV-2 compared to SARS COV-1 (Campitelli et al. 2022). Furthermore, previous studies have shown that allosteric inter-chain communication is important to S protein function (Zhou et al. 2020; Spinello et al. 2021; Tan et al. 2022; Xue et al. 2022). In support of these findings, we observe through DCI_{asym} that when the S protein is in its pre-fusion conformation with one chain open, the CAPs in the closed chains have negative coupling asymmetry with respect to the hACE2 binding site interface in the RBD-open chain. This indicates an allosteric control where the hACE2 binding site is dominated by the dynamics of the CAPs in closed chains (Figure 2B, yellow bars). As this open-state RBD is critical for the viral infection of host cells (Kirchdoerfer et al. 2016), our results suggest that this type of closed-to-open cross-chain interaction is important for viral proliferation. Our prior studies on DCI_{asym} show a similar trend in Lactose Inhibitor (LacI), a protein with a functional role in gene expression through binding DNA. The allosteric mutations (i.e., mutations on the sites that are far from the DNA binding sites) that alter DNA

206   binding affinity not only exhibited unique asymmetry profiles with the DNA binding sites of LacI, but also

207   regulated the dynamics of these binding sites (Campitelli et al. 2020b).

208   Similarly, it is possible that mutations to such residue positions within the S protein can be used to regulate

209   the dynamics of the hACE2 bindings sites of the open RBD state. We, therefore, propose that the residue

210   positions with CAP substitutions hold the potential for mutations in the spike sequence which can alter

211   the opening and closing dynamics of the RBD domain. This hypothesis is further supported by many

212   mutations already observed at these residue positions which alter the infection rate (Brister et al. 2015).

213   Interestingly, residues responsible for extremely low asymmetry values (< -4) lie overwhelmingly in the

214   region 476–486. These same residues were suggested to stabilize S protein dynamics and prime it for host

215   Furin proteolysis (Raghuvamsi et al. 2021).

216   Moreover, as a control, we performed the same analysis on the S protein with the RBD domains of all

217   chains in the closed configuration. In this case, we observed that the DCI_{asym} of the CAPs residue positions

218   with respect to the hACE2 interface in the other chains yields a largely symmetric distribution about 0

219   (Figure 2B, green bars). This verifies that the asymmetry in the coupling of CAPs with the exposed binding

220   site interface in pre-fusion configuration results from one of the RBDs opening up and further suggests

221   the allosteric role played by CAPs in locking the S protein in the RBD open state.

222

223   **Dynamic analysis shows that rigid sites tend to be more highly conserved than flexible sites.**

224   CAPs represent important S protein amino acid changes between related coronaviruses across multiple

225   species and the Wuhan-Hu-1 reference sequence (MN908947). Since SARS-CoV-2 first spread to humans,

226   it has continued to mutate and evolve rapidly, particularly regarding the S protein (Amicone et al. 2022;

227   Liu et al. 2022; Tay et al. 2022). Like the mutations leading to the Wuhan strain caused an increase in

228   binding affinity to hACE2, continued evolution in human hosts has resulted in further altered binding

229 affinities as well as different phenotypic outcomes for those infected (Ali et al. 2021; Barton et al. 2021;

230 Ozono et al. 2021).

231 We explore whether protein dynamics has played a role in the selection of mutational sites during the

232 evolution of the S protein since 2019. Our previous work has indicated that rate of evolution per positional

233 site exhibits a positive correlation with positional flexibility; generally, positions that exhibit higher

234 flexibility are also sites that experience a higher number of amino acid substitutions (Liu and Bahar 2012;

235 Maguid et al. 2008; Maguid et al. 2006; Mikulska-Ruminska et al. 2019; Nevin Gerek, Z., Kumar, S., Banu

236 Ozkan, S. 2013). To confirm these findings for the evolution of the S protein using the sequenced variants

237 of infected humans, we analyze the site-specific amino acid flexibility using the Dynamic Flexibility Index

238 (DFI). Using the same mathematical foundation as DCI, DFI evaluates each position's displacement

239 response to random force perturbations at other locations in the protein (Gerek and Ozkan 2011; Nevin

240 Gerek, Z., Kumar, S., Banu Ozkan, S. 2013), and it can be considered a measure of a given position's ability

241 to explore its local conformational space. We found that the covid-19 S protein shows the expected high

242 correlation between the occurrence of mutations and site flexibility (Figure 3) when we compare %DFI

243 (DFI ranked by percentile) to the average number of variants per position found within a given %DFI bin.

244 Previous studies have indicated that rigid residues are critical for functional dynamics, thus more likely to

245 impact function if mutated and, generally, can lead to a loss of function and thus more conserved (Kim,

246 H. et al. 2015; Butler et al. 2018; Modi, Risso, et al. 2021; Modi, Campitelli, et al. 2021; Kazan et al. 2022;

247 Ose, Butler, et al. 2022; Stevens et al. 2022; Campitelli et al. 2020a; Kumar, A., Glembo, T.J., Ozkan, S.B.

248 2015b). This analysis also agrees with these previous studies and highlights the power of negative

249 selection, in line with the neutral theory of molecular evolution, stating that deleterious mutations (i.e.,

250 those on the rigid positions) should be eliminated and therefore not observed (Kimura, Motoo 1983).
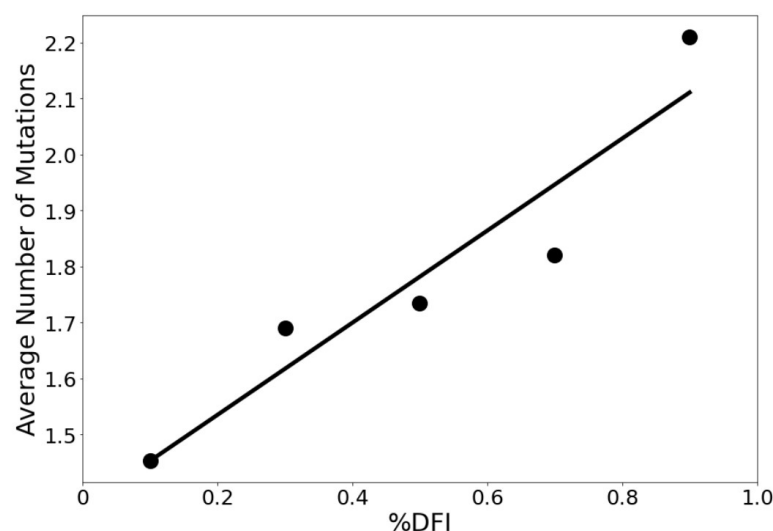
251

Figure 3. The average number of variants observed among residues of different flexibility. Residues were sorted into one of five bins based on flexibility. After that, the average number of variants for residues within that bin was calculated. Here, the number of variants is defined as the number of different amino acid varieties found at that site. Mutational data was calculated across approximately 24,000 SARS-CoV-2 S protein sequences from the NCBI Datasets Project (Brister et al. 2015). Residue flexibility, as reported here via %DFI, was computed using structure id 6vsb from the Protein DataBank (Berman, H.M. et al. 2000). More rigid residues tend to have fewer variants. ($r = 0.94$).

Continued mutations within human hosts have resulted in a multitude of variants. Indeed, by fitting various molecular clock models to genome sequence data, VOC emergence is punctuated by an episodic period of rapid evolution, with a substitution rate of up to 4-fold greater than the background substitution rate (Kumar et al. 2021; Tay et al. 2022). With such an aggressive evolutionary rate, we are finding VOCs to consist of a number of different characteristic mutations, almost all of which are CAPs.

To explore the dynamic effects of the evolution of the Spike in humans, we examine asymmetry with these new potentially adaptive sites, namely the low EP (CAP) characteristic mutation sites observed in the Delta variant, the widely dominant variant from December 2021 to January 2022 (Thye et al. 2021), and the Omicron variant, a highly transmissible variant whose lineages have remained dominant since January 2022) (Kim et al. 2021) (Figure 4). This analysis revealed a mechanism similar to that for the CAPs in the

269   reference protein (Figure 2), as the open-chain binding interface is also allosterically controlled by these

270   potentially new adaptive sites. Regarding this, we see that the asymmetry is much more pronounced in

271   observed mutations of Omicron variants suggesting that these new mutations have a stronger power in

272   controlling the dynamics of open chain hACE2 binding interface compared to those observed in Delta

273   variants. We can speculate that the difference in virulence and infection rates between Omicron and Delta

274   (Earnest et al. 2022; Bager et al. 2021; Sheikh et al. 2021; Twohig et al. 2022;(Houhamdi et al. 2022; Menni

275   et al. 2022) might be due to these specific CAPs within each variant and their differences in allosterically

276   controlling the dynamics of open RBD binding sites as observed in the DCI_{asym} analysis.
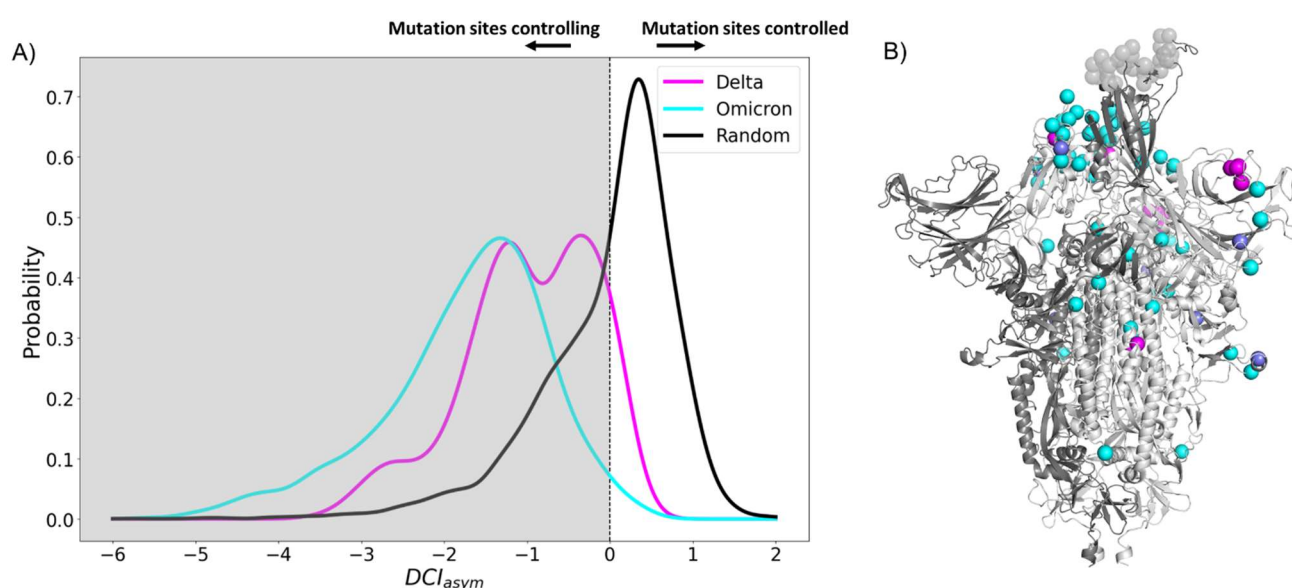

277

278   **Figure 4**. (A) DCI asymmetry with low EP characteristic mutation sites of Delta or Omicron strains in the

279   closed chains and the binding interface of RBD in the open chain. Delta displays a second peak closer to

280   zero, suggesting that Delta mutation sites (M = -0.98, SD = 0.80) have less allosteric control over the

281   hACE2 binding sites than Omicron mutation sites (M = -1.74, SD = 1.00) (p < .001). However, both sets

282   of sites have far more control over hACE2 binding sites than expected, based on a random control group

283   (M = 0.03, SD = 0.85) (p < .001). (B) S protein structure showing binding interface sites (transparent gray),

284   Delta mutation sites (magenta), Omicron mutation sites (cyan), and sites mutated in both Omicron and

285   Delta (Blue).

286

Experimental results motivate the use of EpiScore within the SARS-CoV-2 Spike protein.

The fact that the identified CAPs in the reference protein and the more recently evolved CAPs of Delta and Omicron variants both show a high degree of control over the active sites begs the question: what is the complex interaction between these previous and new CAP sites? Motivated by this concept, we explore the interplay of mutational pairs to understand the effects of the specific amino acid backgrounds associated with these two predominant variants. Some CAP sites in Delta and Omicron have already been considered adaptive (Kemp et al. 2021; Kistler et al. 2022; Maher et al. 2022; Neher 2022).

It is well understood that the impact of even a single mutation to a protein sequence can sometimes dramatically alter the biophysical behavior of the system. However, the mechanistic impact of point mutations can only be fully understood when the sequence background upon which it is made is accounted for. This means that, in the case of strains with multiple mutations, the interplay between mutated positions will ultimately impact a protein as an aggregate behavior, where the presence of previous mutations may strongly (or weakly) influence some mutations. This concept of non-additivity is known as epistasis. In fact, studies of evolutionary pathways of mutations have suggested that a majority of the mutations have a second or a higher order epistasis among them (Bershtein et al. 2006). Nature exploits this higher order complex relationship between the mutations to evolve their function.

To computationally capture and interpret the pairwise effects of mutations, we have developed an in-house computational tool called EpiScore (Figure 5A). Here, we evaluate how a given position pair $i\,j$ may affect other critical positions k of the protein. EpiScore is the relative coupling strength to a position k when positions i and j are perturbed *simultaneously* compared to the average dynamic coupling strength of i to k and j to k. EpiScore has previously been used successfully to capture overarching trends in GB1 deep mutational scan data as well as specific instances of the development of antibiotic resistance in various enzymatic systems (Campitelli and Ozkan 2020). An EpiScore of 1 indicates perfect coupling additivity, and deviations from this value represent non-additive behavior between position pairs and

311 functionally important sites. Prior EpiScore work has shown a difference in EpiScore between the sites of

312 compensatory and non-compensatory mutations, where both yield distributions with peaks around 1, but

313 non-compensatory mutations show higher deviation in their EpiScore distribution (Ose, Campitelli, et al.

314 2022).

315 Many studies have confirmed epistasis between residues within the S protein (Moulana et al. 2022a; Starr,

316 Greaney, Hannon, et al. 2022; Moulana et al. 2023; Witte et al. 2023). These epistatic residues can have

317 various effects on hACE2 or antibody binding. To further motivate our use of EpiScore within SARS-CoV-

318 2, we calculate the EpiScore (Figure 5B) of a set of mutation pairs used by Moulana et al. (Nature comm

319 2022) and compare our results to quantified epistatic effects determined by the experimental hACE2

320 binding affinity of "first-order" single mutation variants compared to "second-order" mutation pair. Our

321 EpiScore results and the experimentally determined epistasis have a reasonable similarity. Both methods

322 captured highly epistatic behavior among residues 493, 496, 498, 501, and 505, as well as a lack of epistatic

$$\text{EpiScore:} \quad \frac{\%DCI_{[ij]k}}{\frac{1}{2}(\%DCI_{ik} + \%DCI_{jk})}$$
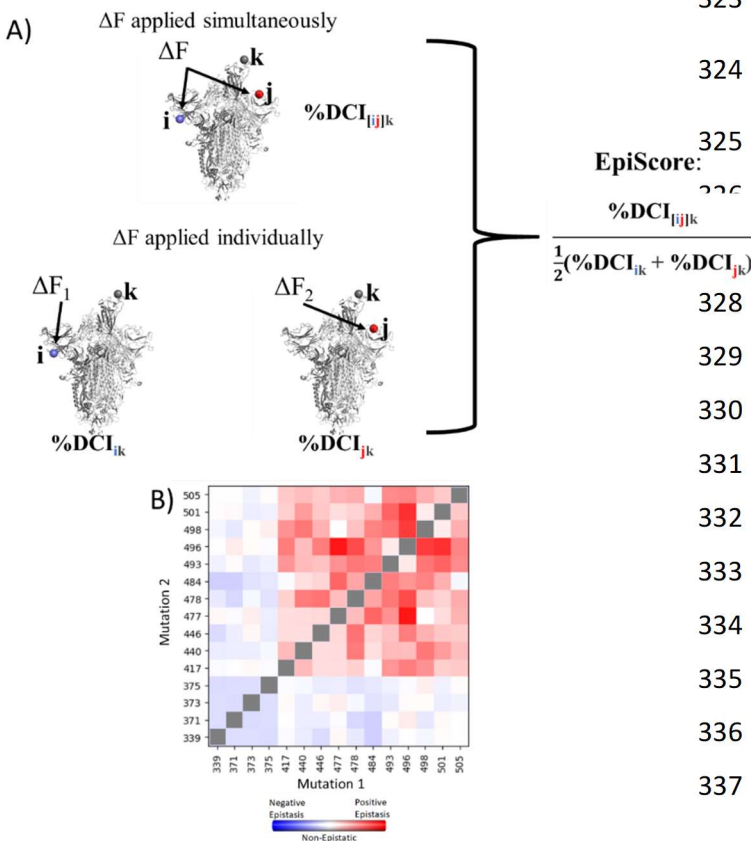
323 behavior for residues 339, 371, 373,

324 and 375.

325 **Figure 5.** (A) Schematic

326 representation of cross-chain

327 EpiScore, describing i, j, in chain B and

328 C respectively and its impact in RBD

329 binding position k in the open RBD

330 conformer chain A. (B) Colors indicate

331 EpiScore values for given mutation

332 pairs, averaged over hACE2 binding

333 sites. Cross-chain residue pairs in the

334 upper right tend to be highly

335 epistatic, similar to pairwise second-

336 order interaction coefficients from

337 Moulana et al. (Nature comm 2022).

338   **Episcore highlights the epistatic relationship between the recent adaptive mutations in VOCs and the**

339   **CAPs of the Wuhan reference.**

340   Seeking further to understand the role of epistasis within S protein variants, we explored the possibility

341   of epistatic relationships between the CAPs of the Wuhan variant and the new CAPs in VOCs. Thus, we

342   computed the Episcore of these CAP positions in the closed RBD domains (i.e., chain B and C) with respect

343   to functional hACE2 binding interface sites of the open RBD domain chain (chain A) (Figure 5B) and

344   obtained Episcore distributions.
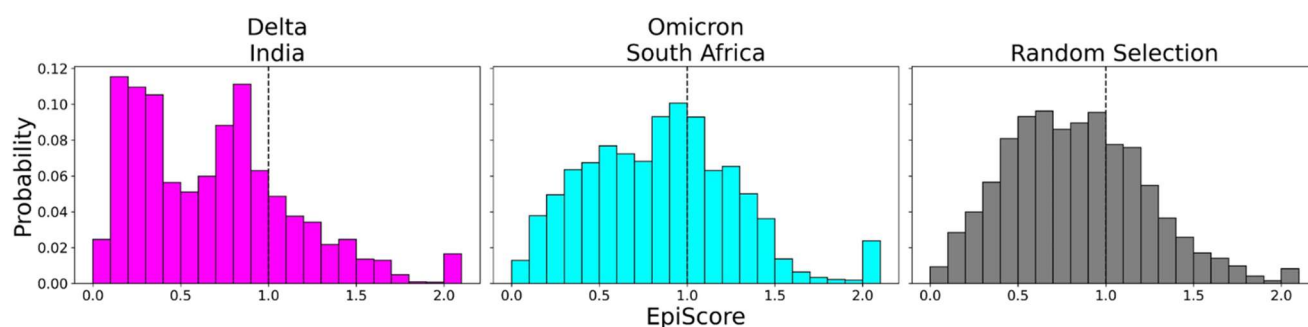
345

346

347   **Figure 6**. EpiScores with I = low EP Delta mutation sites (magenta), low EP Omicron mutation sites (Cyan),

348   and a random selection of sites (gray), j = low EP sites in the Wuhan variant, and k = the binding interface

349   of the open chain. EpiScores using sites of either variant (Delta: M = 0.70, SD = 0.50, Omicron M = 0.86,

350   SD = 0.46) are significantly different (p<.001) from a set of EpiScores using random sites (M = 0.84, SD =

351   0.41), but the distribution for Delta variants differs much more from the other two. EpiScores for other

352   variants can be found in Supplementary Figure S1.

353

354   To contrast these variants, Omicron (Figure 6, cyan) shows a high proportion of additive, potentially

355   compensatory, mutations compared to the Delta variant (Figure 6, magenta), with a peak centered on 1.

356   The comparatively more pathogenic Delta variant exhibited many non-additive, suspected non-

357   compensatory mutations with EpiScores below one. This again suggests that the cross-communication

358   between the open and closed chain of the S protein is important for regulating the function. Four out of

359   seven low EP Delta mutation sites used in this analysis often resulted in EpiScores below 1. Each of those

360   is found in the N-terminal domain (NTD) on or near the N3 loop and is implicated in antibody escape in

361   recent studies (Chi et al. 2020; Weisblum et al. 2020; Harvey, Carabelli, Jackson, Gupta, Thomson,

362   Harrison, Ludden, Reeve, Rambaut, COVID-19 Genomics UK (COG-UK) Consortium, et al. 2021; Klinakis et

363   al. 2021; Cantoni et al. 2022). The low EpiScores of NTD mutations suggest that they dampen the control

364   of Wuhan variant CAPs over the active site in addition to their effects on antibody binding. It is possible

365   that what the Delta variant gained in transmission rate also came with being more harmfully pathogenic

366   due in part to negatively epistatic interactions. It follows that the mutations leading to the development

367   of the Omicron strain were compensatory in nature, possibly leading to a lower pathogenicity and higher

368   effective immune escape, resulting in a higher transmission rate. It is worth noting that other variants

369   contain NTD mutations which result in low EpiScores, however the proportion of these mutations within

370   the set is considerably less than in Delta (Supplementary Figure S2).

371   One of the more notable similarities of generated EpiScore distributions is a tail of EpiScore values upward

372   of 2.0, indicating highly epistatic behavior. Interestingly, these tails are largely due to three different CAPs:

373   346R, 486F, and 498Q. Those residues are nearby one another within the protein structure and have been

374   reported to play a role in antibody binding, either being known antibody binding sites (346R and 486F) or

375   having received very high antibody accessibility scores (498Q) (Harvey, Carabelli, Jackson, Gupta,

376   Thomson, Harrison, Ludden, Reeve, Rambaut, COVID-19 Genomics UK (COG-UK) Consortium, et al. 2021;

377   Raghuvamsi et al. 2021). These observed high Episcore values also support the other studies that the

378   epistatic interactions between these CAPs and the mutations of the VOCs within the S protein are crucial

379   for maintaining binding affinity of hACE2 whilst evading immunity (Hong et al. 2022; Moulana et al. 2022b;

380   Starr, Greaney, Stewart, et al. 2022).

381   Viewing EpiScores of Delta and Omicron potentially adaptive mutation sites with only CAP site 486F (a

382   binding site for both hACE2 and antibodies) (Huang et al. 2020; Ali et al. 2021; Harvey, Carabelli, Jackson,

383   Gupta, Thomson, Harrison, Ludden, Reeve, Rambaut, COVID-19 Genomics UK (COG-UK) Consortium, et

384   al. 2021; Raghuvamsi et al. 2021) shows highly epistatic interactions at other hACE2 binding sites (Figure

385   6). However, within a recent and rapidly spreading subvariant of Omicron, XBB 1.5, we see a mutation of

386   F to S, a rare double nucleotide mutation, at site 486. This new variant has unprecedented immune escape

387   capabilities, resisting neutralizing antibodies almost entirely (Qu et al. 2023). EpiScores of other XBB 1.5

388   specific mutation sites with 486S are almost entirely greater than 1, showing an even higher degree of

389   epistasis with the binding sites of RBD (Figure 7). These results present a threefold importance for the

390   F486S mutation: Not only does this residue alter antibody (i.e., immune escape) and hACE2 binding by

391   directly modifying a binding site, but it may also be responsible for modifying hACE2 binding via epistatic

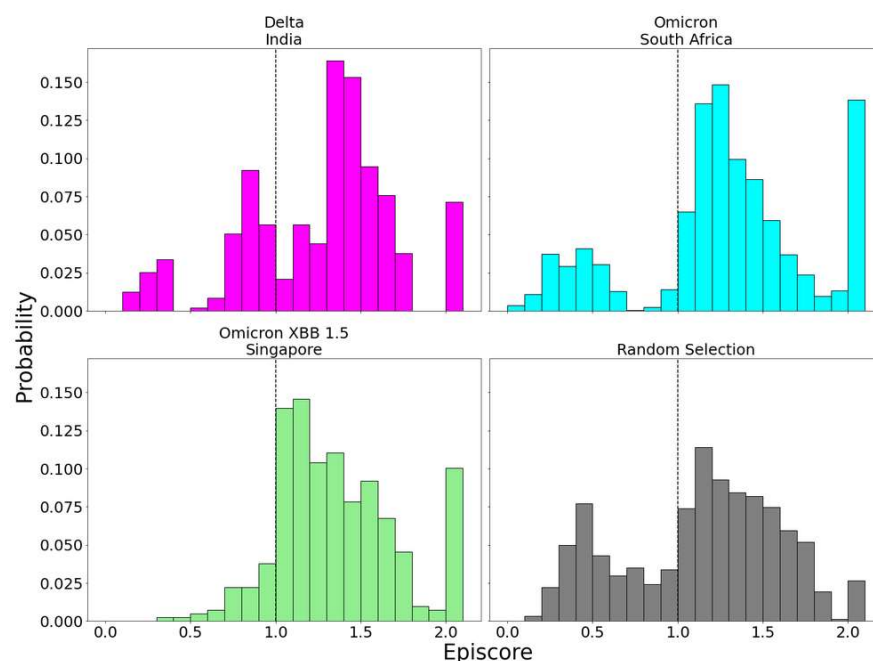392   cooperation with other co-occurring mutations.

Figure 7. EpiScores with i = low EP Delta mutation sites (magenta), low EP Omicron mutation sites (Cyan), and a random selection of sites (gray), j = site 486, and k = the binding interface of the open chain. CAP and hACE2 and antibody binding site 486 displays epistasis with almost all XBB 1.5 variant

405   sites at almost every hACE2

406   binding site (M = 1.40, SD = 0.46) and presents a significantly different profile from other variant sites (p

407   <.01). EpiScores involving 486 for other variants can be found in Supplementary Figure S1.

408

409 **Change in flexibility of RBD binding site correlates with experimental binding affinities for Omicron and**

410 **Omicron XBB variants.**

411 Experimental studies have tracked hACE2 binding for different variants since the virus first spread (Ali et

412 al. 2021; Barton et al. 2021; Ozono et al. 2021; Wu et al. 2022). Within the Omicron variant, for example,

413 characteristic mutations on the RBD are shown to increase the overall binding affinity of the virus to the

414 ACE2 receptor, which is suspected to allow it to spread more easily (Kim et al. 2021). Furthermore, the

415 new Omicron XBB and Omicron XBB 1.5 variants contain additional mutations in the RBD and antibody

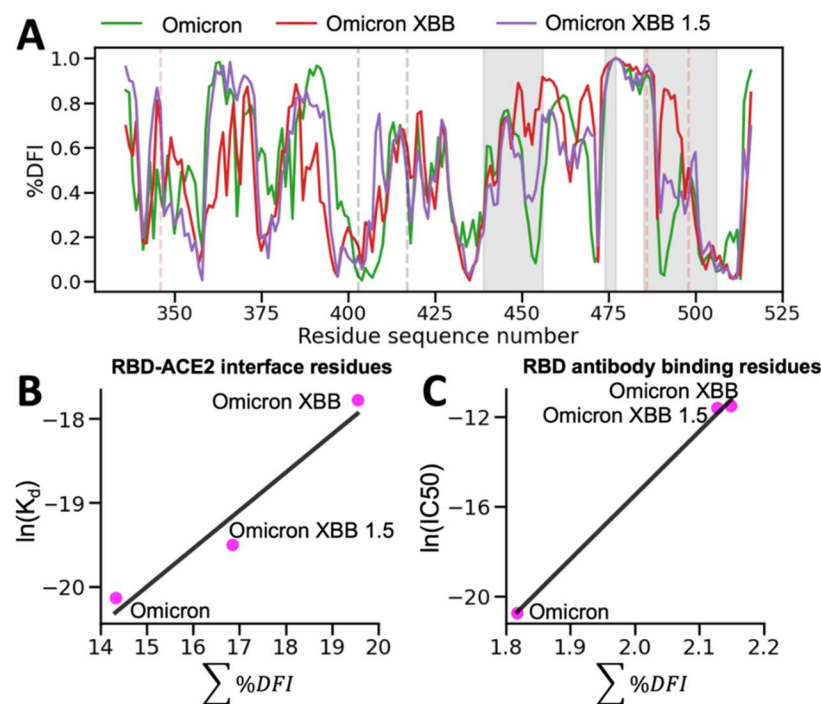416 binding residues, which may further impact their dynamics and interactions with the host.

417

418

419 **Figure 8.** The %DFI calculations for variants Omicron, XBB, and XBB 1.5. (A) %DFI profile of the variants

420 are plotted in the same panel. The grey shaded areas and dashed lines indicate the ACE2 binding regions,

421 whereas the red dashed lines show the antibody binding residues. (B) The sum of %DFI values of RBD-

422 ACE2 interface residues. The trend of total %DFI with the log of K_d values overlaps with the one seen with

423 the experiments (R=0.97). (C) The RBD antibody binding residues are used to calculate the sum of %DFI.

424 The ranking captured with the total %DFI agrees with the log of IC50 values from the experiments.

425   To gain deeper insights into the impact of dynamics on the binding affinity of hACE2 and antibodies with

426   the recent Omicron XBB variants, we conducted molecular dynamics (MD) simulations. By analyzing the

427   resulting trajectories, we investigated how these mutations influence the flexibility and rigidity of the RBD

428   and antibody binding residues, consequently affecting their binding affinity and potential for immune

429   evasion (Figure 8). To understand the overall flexibility changes, we measured the sum of DFI of the ACE2

430   binding residues, as well as the sum of DFI of the antibody binding residues, calculated from the MD

431   trajectories and compared then with experimental viral binding (disassociation constants) and immunity

432   evasion antibody IC50 values (Yue et al. 2023).

433   This investigation elucidated the impact of mutations in the receptor-binding domain (RBD) and antibody

434   binding residues on the binding affinity of the S protein and immune evasion by modulating their flexibility

435   and rigidity (Figure 8A). The Omicron XBB variant exhibits heightened flexibility in hACE2 and antibody

436   binding residues, reducing infectivity and enhancing immune evasion. Conversely, the Omicron XBB 1.5

437   variant induces distinct dynamics in these regions, rendering the RBD-ACE2 interface more rigid while

438   increasing flexibility in antibody binding residues. These effects indicate that Omicron XBB1.5 retains its

439   antibody escape capabilities while regaining ACE2 binding affinity comparable to previous Omicron

440   variants, in accordance with experimental findings (Yue et al. 2023). These findings suggest that mutations

441   in the RBD and antibody binding residues can have complex effects on the dynamics of the protein and,

442   ultimately, on the virus's ability to infect and evade the host immune system through an alteration of

443   biding site dynamics.

444

445   **Conclusion:**

446   We analyzed the evolutionary trajectory of the CoV-2 S protein in humans to understand the dynamic

447   and epistatic interactions of the mutations defining specific VOCs within the S protein. We first obtain

448   the phylogenetic tree of the COV-2 S protein and identify the sites of certain recent mutations known as

449   candidate adaptive polymorphisms (CAPs). CAPs are considered adaptive because mutations rarely

450   tolerated in closely related sequences have suddenly become fixed, implying a degree of functional

451   importance or evolution (Liu et al. 2016). In addition, our earlier work has shown that CAPS can also be

452   compensatory as multiple CAPs may dynamically compensate for one another, changing the dynamic

453   landscape and allowing for different mutations (Ose, Campitelli, et al. 2022). We then explored the

454   mechanistic insights and epistatic relationship between the observed mutations in different VOCs and

455   the CAP sites, and, particularly, the relationship between CAP sites and the functionally critical RBD

456   domain using our dynamic coupling analysis (Kumar, A., Glembo, T.J., Ozkan, S.B. 2015b).

457   We find a mechanistic pattern in the S protein evolution that is common amongst previously studied

458   systems, where allosteric sites exert control over the dynamics of the active site, and mutations of these

459   allosteric sites modulate function. Within the S protein, these critical regulatory sites are CAPs and VOC-

460   defining new putative adaptive mutations. However, this regulation is significantly less in Delta-defining

461   mutations than in the Omicron variant. We speculate that this may cause some differences in behavior

462   between the strains. Simply looking at the connection between hACE2 binding and pathogenicity, we

463   know that the Omicron variant is less pathogenic and has a lower binding affinity (Wu et al. 2022) than

464   previous variants. Our dynamics analysis provides a mechanistic insight where the Omicron defining

465   sites have greater control over the active sites than the Delta variant, and compensate for the functional

466   advantage of CAPs, thus, the greatest infectivity may not be a coincidence.

467   Specifically, we find that the interactions between CAP sites and VOC-defining mutations show

468   fingerprints of non-compensatory dynamics within the Delta variant. In contrast, mutations leading to

469   the Omicron variant are largely compensatory, driving critical dynamical behavior closer to the patterns

470   observed within the wild-type. These interactions may drive observed behavior similar between the

471   reference and Omicron strains yet differ in the delta strain, such as the severity of infection as evidenced

472   by hospitalization rates (Houhamdi et al. 2022; Menni et al. 2022).

473   Long-ranged interactions between different sites within a given protein is critically important for protein

474   function (Peters and Lively 1999; Bershtein et al. 2006; Collins et al. 2006; Ekeberg et al. 2013; Levy et al.

475   2017; Harrigan et al. 2018; Otten et al. 2018; Rojas Echenique et al. 2019; Shimagaki and Weigt 2019; de

476   la Paz et al. 2020; Rizzato et al. 2020; Yang et al. 2020; Bisardi et al. 2022) and for the CoV-2 S protein in

477   particular (Zeng et al. 2020; Castiglione et al. 2021; Dong et al. 2021; Garvin et al. 2021; Nielsen et al.

478   2022; Ramarao-Milne et al. 2022; Rochman et al. 2022; Rodriguez-Rivas et al. 2022). By showing dynamic

479   differences between the interactions of CAPs, which have likely played a major role in allowing the virus

480   to infect human hosts, the binding site, and the characteristic mutations of dominant Delta and Omicron

481   strains, we see a "fine-tuning" of protein behavior. As variants continue to evolve, Omicron sub-variants

482   are of growing concern due in large part to further increased immune evasion (Callaway 2022; Wang, Guo,

483   et al. 2022; Wang, Iketani, et al. 2022), and we observe that the new mutations observed in antibody

484   binding sites yield more epistatic interaction with the CAPs. In addition to supporting previous dynamic

485   research on the S protein, this analysis provides the insight that CAP sites are of continued importance to

486   protein function and should be given special attention when considering the impact of future mutations.

487

488   **Methods**

489

490   **Dynamic Flexibility and Dynamic Coupling**

491   The Dynamic Flexibility Index utilizes a Perturbation Response Scanning technique that combines the Elas-

492   tic Network Model (ENM) and Linear Response Theory (LRT) (Gerek and Ozkan 2011; Nevin Gerek, Z.,

493   Kumar, S., Banu Ozkan, S. 2013). In ENM, the protein is considered as a network of beads at Cα positions

494   interacting with each other via a harmonic spring potential. Using LRT, Δ**R** is calculated as the fluctuation

495   response vector of residue j due to unit force's **F** perturbation on residue $i,$ averaged over multiple unit

496   force directions to simulate an isotropic perturbation.

497

$$[\Delta \mathbf{R}]_{3N \times 1} = [\mathbf{H}]^{-1}_{3N \times 3N} [\mathbf{F}]_{3N \times 1}$$

(1)

500　**H** is the Hessian, a 3N × 3N matrix that can be constructed from 3-D atomic coordinate information and is

501　composed of the second derivatives of the harmonic potential with respect to the components of the

502　position's vectors of length 3N. The hessian inverse in this equation may be replaced with the covariance

503　matrix **G** obtained from MD simulations as follows.

504

$$[\Delta \mathbf{R}]_{3N \times 1} = [\mathbf{G}]_{3N \times 3N} [\mathbf{F}]_{3N \times 1}$$

(2)

507　MD simulations were used to obtain the DFI profiles of Omicron, Omicron XBB, and Omicron XBB 1.5. In

508　order to obtain DFI, each position in the structure was perturbed sequentially to generate a Perturbation

509　Response Matrix *A*

510

$$\mathbf{A}_{N \times N} = \begin{bmatrix} |\Delta R^1|_1 & \cdots & |\Delta R^N|_1 \\ \vdots & \ddots & \vdots \\ |\Delta R^1|_N & \cdots & |\Delta R^N|_N \end{bmatrix}$$

(3)

513　where $\left|\Delta R^j\right|_i = \sqrt{\langle(\Delta R)^2\rangle}$ is the magnitude of fluctuation response at position *i* due to perturbations at

514　position *j*. *T*he DFI value of position *i* is then treated as the displacement response of position *i* relative to

515　the net displacement response of the entire protein, which is calculated by sequentially perturbing each

516　position in the structure.

517

519
$$\text{DFI}_i = \frac{\sum_{j=1}^{N}\left|\Delta R^j\right|_i}{\sum_{i=1}^{N}\sum_{j=1}^{N}\left|\Delta R^j\right|_i}$$

518   (4)

520   It is also often useful to quantify position flexibility relative to the flexibility ranges unique to individual

521   structures. To that end, DFI can be presented as a percentile rank, %DFI. All %DFI calculations present in

522   this work used the DFI value of every residue of the full spike structure for ranking. The DFI parameter can

523   be considered a measure of a given amino acid position's ability to explore its local conformational space.

524

525   **Dynamic Coupling Index**

526   Similar to DFI, the dynamic coupling index (DCI) (Larrimore et al. 2017; Kumar, A., Glembo, T.J., Ozkan,

527   S.B. 2015b) also utilizes Perturbation Response Scanning with the Elastic Network Model and Linear

528   Response Theory. DCI captures the strength of displacement response of a given position *i* upon

529   perturbation to a single functionally important position (or subset of positions) *j*, relative to the average

530   fluctuation response of position *i* when all of the positions within a structure are perturbed.

531

534
$$\text{DCI}_{ji} = \frac{\sum_{j}^{N_{functional}}\left|\Delta R^j\right|_i / N_{functional}}{\sum_{j=1}^{N}\left|\Delta R^j\right|_i / N}$$

532   (5)

533   When only positional pairs are concerned, this expression reduces to:

535

537
$$\text{DCI}_{ji} = \frac{\left|\Delta R^j\right|_i}{\sum_{j=1}^{N}\left|\Delta R^j\right|_i / N}$$

536   (6)

538   As such, this parameter represents a measure of the dynamic coupling between i and j upon a

539   perturbation to j. As with DFI, DCI_{ji} can also be presented as a percentile-ranked $\%DCI_{ji}$.

540   One of the most important aspects of DCI is that the entire network of interactions is explicitly included

541   in subsequent calculations without the need for dimensionality reduction techniques. If one considers

542   interactions such as communication directionality or dynamic coupling regulation between position pairs

543   as inherent properties of an anisotropic interaction network, it is critical to include the interactions of the

544   entire network to accurately model the effect one residue can have on another.

545   Here, we present two further extensions of DCI which allow us to uniquely model coupling directionality

546   and epistatic effects: DCI_{asym} and EpiScore, respectively. Interestingly, we can capture asymmetry between

547   different residues within a protein through DCI, as a coupling in and of itself is asymmetric within an ani-

548   sotropic network. That is, each amino acid has a set of positions to which it is highly coupled, and this

549   anisotropy in connections gives rise to unique differences in coupling between a given $i\,j$ pair of amino

550   acids which do not have direct interactions (Figure 2A). DCI_{asym}, then, is simply DCI_{ij} (the normalized dis-

551   placement response of position j upon a perturbation to position i) – DCI_{ji} (Equation (7)). Using DCI_{asym} we

552   can determine a cause-effect relationship between the $i\,j$ pair in terms of force/signal propagation be-

553   tween these two positions.

554

556    $$DCI_{asym} = DCI_{ij} - DCI_{ji}$$

555   (7)

558    $$\%DCI_{asym} = \%DCI_{ij} - \%DCI_{ji}$$

557   (8)

559   where a positive DCI_{asym} value indicates communication from position i to position j.

560   EpiScore can identify or describe potential non-additivity in substitution behavior between residue pairs.

561   This metric can capture the differences in a normalized perturbation response to a position k when a force

562   is applied at two residues i and j simultaneously versus the average additive perturbation response when

563   each residue i, j, is perturbed individually (Figure 5A, Equation 9).

566

$$EpiScore = \frac{\%DCI_{[ij]k}}{\frac{1}{2}\left(\%DCI_{ik} + \%DCI_{jk}\right)}$$

564

565   (9)

567

568   EpiScore values < 1 (> 1) indicate that the additive perturbations of positions i and j generates a greater

569   (lesser) response at position k than the effect of a simultaneous perturbation. This means that, when

570   treated with a simultaneous perturbation at both sites i and j, the displacement response of k is lower

571   (higher) than the average effect of individual perturbations to i and j, one at a time. As EpiScore is a linear

572   scale, the further the value from 1, the greater the effect described above.

573   **Molecular Dynamics (MD)**

574   The production simulations of the variants Omicron, Omicron XBB, and Omicron XBB 1.5 were generated

575   using the AMBER software package. The mutations in the variants were modeled using PYMOL taking the

576   template as PDB 6M0J. The initial input proteins were parametrized utilizing the ff14SB force field (Maier

577   et al. 2015). To ensure adequate solvation of the protein, the solvation box was defined to encompass the

578   protein, maintaining a minimum distance of 16Å from the protein to the box edges, utilizing the explicit

579   TIP3P water model (Sun 1995). The neutralization of the solvated system was achieved through the addi-

580   tion of sodium and chloride ions. The system was subjected to a steepest descent algorithm for 11000

581   steps for minimization purposes. The minimized system was then heated to 300K and subjected to a con-

582   stant number of particles, pressure, and temperature ensemble (NPT) production simulations. These sim-

583   ulations were conducted using the Langevin thermostat (Hünenberger 2005) and Berendsen barostat

584   (Berendsen et al. 1984). The hydrogens were constrained using the SHAKE algorithm (Pearlman et al.

585   1995). The production trajectories were simulated for 1μs at 300K and 1 bar.

586

587   **Data and Resource Availability**

588   The code to perform DFI and DCI analysis is available at https://github.com/SBOZKAN/DFI-DCI.

589   Molecular Dynamics data are available upon request. The mutation sites and EP values are contained in

590   the supporting information files as "Supplementary_mutation_info.csv". The alignment used to

591   generate EP values is also contained within the supporting information files as "EP_alignment.fas".

592   Protein Databank ID number 6VXX (Walls et al. 2020) was used for closed conformation DCI calculations.

593   6VSB (Wrapp et al. 2020) was used for DFI calculations, EpiScore calculations, and open conformation

594   DCI calculations. 6M0J (Lan et al. 2020) was used in molecular dynamics simulations of the RBD.

595   **Acknowledgements**

600   **References:**

601   Ali F, Kasry A, Amin M. 2021. The new SARS-CoV-2 strain shows a stronger binding affinity to ACE2 due
602   to N501Y mutant. *Med. Drug Discov.* 10:100086.

603   Amicone M, Borges V, Alves MJ, Isidro J, Zé-Zé L, Duarte S, Vieira L, Guiomar R, Gomes JP, Gordo I. 2022.
604   Mutation rate of SARS-CoV-2 and emergence of mutators during experimental evolution. *Evol.*
605   *Med. Public Health* 10:142–155.

606   Barton MI, MacGowan SA, Kutuzov MA, Dushek O, Barton GJ, van der Merwe PA. 2021. Effects of
607   common mutations in the SARS-CoV-2 Spike RBD and its ligand, the human ACE2 receptor on
608   binding affinity and kinetics. *eLife* 10:e70658.

609   Berendsen HJC, Postma JPM, van Gunsteren WF, DiNola A, Haak JR. 1984. Molecular dynamics with
610   coupling to an external bath. *J. Chem. Phys.* 81:3684–3690.

611   Berman, H.M., Westbrook, J., Feng, Z., Gilliland, G., Bhat, T.N., Weissig, H., Shindyalov, I.N., Bourne, P.E.
612   2000. The Protein Data Bank. *Nucleic Acids Res* 28:235–242.

613   Bershtein S, Segal M, Bekerman R, Tokuriki N, Tawfik DS. 2006. Robustness–epistasis link shapes the
614   fitness landscape of a randomly drifting protein. *Nature* 444:929–932.

615   Bhabha G, Ekiert DC, Jennewein M, Zmasek CM, Tuttle LM, Kroon G, Dyson HJ, Godzik A, Wilson IA,
616   Wright PE. 2013. Divergent evolution of protein conformational dynamics in dihydrofolate
617   reductase. *Nat. Struct. Mol. Biol.* 20:1243–1249.

618   Bisardi M, Rodriguez-Rivas J, Zamponi F, Weigt M. 2022. Modeling Sequence-Space Exploration and
619   Emergence of Epistatic Signals in Protein Evolution.Ozkan B, editor. *Mol. Biol. Evol.* 39:msab321.

620   Boni MF, Lemey P, Jiang X, Lam TT-Y, Perry BW, Castoe TA, Rambaut A, Robertson DL. 2020. Evolutionary
621   origins of the SARS-CoV-2 sarbecovirus lineage responsible for the COVID-19 pandemic. *Nat.*
622   *Microbiol.* 5:1408–1417.

623   Brister JR, Ako-adjei D, Bao Y, Blinkova O. 2015. NCBI Viral Genomes Resource. *Nucleic Acids Res.*
624   43:D571–D577.

625   Butler BM, Kazan IC, Kumar A, Ozkan SB. 2018. Coevolving residues inform protein dynamics profiles and
626   disease susceptibility of nSNVs.Jernigan RL, editor. *PLOS Comput. Biol.* 14:e1006626.

627   Cagliani R, Forni D, Clerici M, Sironi M. 2020. Computational Inference of Selection Underlying the
628   Evolution of the Novel Coronavirus, Severe Acute Respiratory Syndrome Coronavirus 2.Gallagher
629   T, editor. *J. Virol.* 94:e00411-20.

630   Callaway E. 2022. COVID 'variant soup' is making winter surges hard to predict. *Nature* 611:213–214.

631   Campbell, E., Kaltenbach, M., Correy, G., Carr, P., Porebski, B.T., Livingstone, E., Jurnou, L., Hyvönen, M.,
632   Buckle, A.M., Weik, M., et al. 2016. The role of protein dynamics in the evolution of new enzyme
633   function. *Nat Chem Biol*.

634   Campitelli P, Lu J, Ozkan SB. 2022. Dynamic allostery highlights the evolutionary differences between the
635   CoV-1 and CoV-2 main proteases. *Biophys. J.* 121:1483–1492.

636   Campitelli P, Modi T, Kumar S, Ozkan SB. The Role of Conformational Dynamics and Allostery in
637   Modulating Protein Evolution. *Annu. Rev. Biophys.* 49:267–288.

638   Campitelli P, Modi T, Kumar S, Ozkan SB. 2020a. The Role of Conformational Dynamics and Allostery in
639   Modulating Protein Evolution. *Annu. Rev. Biophys.* 49:267–288.

640   Campitelli P, Ozkan SB. 2020. Allostery and Epistasis: Emergent Properties of Anisotropic Networks.
641   *Entropy* 22:667.

642   Campitelli P, Swint-Kruse L, Ozkan SB. 2020b. Substitutions at Nonconserved Rheostat Positions
643   Modulate Function by Rewiring Long-Range, Dynamic Interactions.Wilke C, editor. *Mol. Biol.*
644   *Evol.* 38:201–214.

645   Cantoni D, Murray MJ, Kalemera MD, Dicken SJ, Stejskal L, Brown G, Lytras S, Coey JD, McKenna J,
646   Bridgett S, et al. 2022. Evolutionary remodelling of N-terminal domain loops fine-tunes SARS-
647   COV -2 spike. *EMBO Rep.* [Internet] 23. Available from:
648   https://onlinelibrary.wiley.com/doi/10.15252/embr.202154322

649   Carabelli AM, Peacock TP, Thorne LG, Harvey WT, Hughes J, COVID-19 Genomics UK Consortium, De
650   Silva TI, Peacock SJ, Barclay WS, De Silva TI, et al. 2023. SARS-CoV-2 variant biology: immune
651   escape, transmission and fitness. *Nat. Rev. Microbiol.* [Internet]. Available from:
652   https://www.nature.com/articles/s41579-022-00841-7

653   Castiglione GM, Zhou L, Xu Z, Neiman Z, Hung C-F, Duh EJ. 2021. Evolutionary pathways to SARS-CoV-2
654   resistance are opened and closed by epistasis acting on ACE2.Hejnol A, editor. *PLOS Biol.*
655   19:e3001510.

656   Chan C-M, Woo PCY, Lau SKP, Tse H, Chen H-L, Li F, Zheng B-J, Chen L, Huang J-D, Yuen K-Y. 2008. Spike
657   Protein, S, of Human Coronavirus HKU1: Role in Viral Life Cycle and Application in Antibody
658   Detection. *Exp. Biol. Med.* 233:1527–1536.

659   Changeux J-P, Edelstein SJ. 2005. Allosteric Mechanisms of Signal Transduction. *Science* 308:1424–1428.

660   Chi X, Yan R, Zhang Jun, Zhang G, Zhang Y, Hao M, Zhang Z, Fan P, Dong Y, Yang Y, et al. 2020. A
661   neutralizing human antibody binds to the N-terminal domain of the Spike protein of SARS-CoV-
662   2. *Science* 369:650–655.

663   Collins SR, Schuldiner M, Krogan NJ, Weissman JS. 2006. A strategy for extracting and analyzing large-
664   scale quantitative epistatic interaction data. *Genome Biol.* 7:R63.

665   Damas J, Hughes GM, Keough KC, Painter CA, Persky NS, Corbo M, Hiller M, Koepfli K-P, Pfenning AR,
666   Zhao H, et al. 2020. Broad host range of SARS-CoV-2 predicted by comparative and structural
667   analysis of ACE2 in vertebrates. *Proc. Natl. Acad. Sci.* 117:22311–22322.

668   Deng X, Garcia-Knight MA, Khalid MM, Servellita V, Wang C, Morris MK, Sotomayor-González A, Glasner
669   DR, Reyes KR, Gliwa AS, et al. 2021. Transmission, infectivity, and antibody neutralization of an
670   emerging SARS-CoV-2 variant in California carrying a L452R spike protein mutation. Infectious
671   Diseases (except HIV/AIDS) Available from:
672   http://medrxiv.org/lookup/doi/10.1101/2021.03.07.21252647

673   Díaz-Salinas MA, Li Q, Ejemel M, Yurkovetskiy L, Luban J, Shen K, Wang Y, Munro JB. 2022.
674   Conformational dynamics and allosteric modulation of the SARS-CoV-2 spike. *eLife* 11:e75433.

675   Dicken SJ, Murray MJ, Thorne LG, Reuschl A-K, Forrest C, Ganeshalingham M, Muir L, Kalemera MD,
676   Palor M, McCoy LE, et al. 2021. Characterisation of B.1.1.7 and Pangolin coronavirus spike
677   provides insights on the evolutionary trajectory of SARS-CoV-2. Microbiology Available from:
678   http://biorxiv.org/lookup/doi/10.1101/2021.03.22.436468

679   Dong A, Zhao J, Griffin C, Wu R. 2021. The Genomic Physics of COVID-19 Pathogenesis and Spread. *Cells*
680   11:80.

681   Doshi U, Holliday MJ, Eisenmesser EZ, Hamelberg D. 2016. Dynamical network of residue–residue
682   contacts reveals coupled allosteric effects in recognition, catalysis, and mutation. *Proc. Natl.*
683   *Acad. Sci.* 113:4735–4740.

684   Dror RO, Dirks RM, Grossman JP, Xu H, Shaw DE. 2012. Biomolecular Simulation: A Computational
685   Microscope for Molecular Biology. *Annu. Rev. Biophys.* 41:429–452.

686   Ekeberg M, Lövkvist C, Lan Y, Weigt M, Aurell E. 2013. Improved contact prediction in proteins: Using
687   pseudolikelihoods to infer Potts models. *Phys. Rev. E* 87:012707.

688   Frost SDW, Magalis BR, Kosakovsky Pond SL. 2018. Neutral Theory and Rapidly Evolving Viral
689   Pathogens.Kumar S, editor. *Mol. Biol. Evol.* 35:1348–1354.

690   Garvin MR, Prates ET, Romero J, Cliff A, Machado Gazolla JGF, Pickholz M, Pavicic M, Jacobson D. 2021.
691   Rapid expansion of SARS-CoV-2 variants of concern is a result of adaptive epistasis. Evolutionary
692   Biology Available from: http://biorxiv.org/lookup/doi/10.1101/2021.08.03.454981

693   Gerek ZN, Ozkan SB. 2011. Change in Allosteric Network Affects Binding Affinities of PDZ Domains:
694   Analysis through Perturbation Response Scanning.Nussinov R, editor. *PLoS Comput. Biol.*
695   7:e1002154.

696   Gobeil SM-C, Janowska K, McDowell S, Mansouri K, Parks R, Manne K, Stalls V, Kopp MF, Henderson R,
697   Edwards RJ, et al. 2021. D614G Mutation Alters SARS-CoV-2 Spike Conformation and Enhances
698   Protease Cleavage at the S1/S2 Junction. *Cell Rep.* 34:108630.

699   Gobeil SM-C, Janowska K, McDowell S, Mansouri K, Parks R, Stalls V, Kopp MF, Manne K, Li D, Wiehe K,
700   et al. 2021. Effect of natural mutations of SARS-CoV-2 on spike structure, conformation, and
701   antigenicity. *Science* 373:eabi6226.

702   Goldman N. 1990. Maximum Likelihood Inference of Phylogenetic Trees, with Special Reference to a
703   Poisson Process Model of DNA Substitution and to Parsimony Analyses. *Syst. Zool.* 39:345.

704   Gur M, Taka E, Yilmaz SZ, Kilinc C, Aktas U, Golcuk M. 2020. Conformational transition of SARS-CoV-2
705   spike glycoprotein between its closed and open states. *J. Chem. Phys.* 153:075101.

706   Harrigan P, Madhani HD, El-Samad H. 2018. Real-Time Genetic Compensation Defines the Dynamic
707   Demands of Feedback Control. *Cell* 175:877-886.e10.

708   Harvey WT, Carabelli AM, Jackson B, Gupta RK, Thomson EC, Harrison EM, Ludden C, Reeve R, Rambaut
709   A, Consortium C-19 GU (COG-U, et al. 2021. SARS-CoV-2 variants, spike mutations and immune
710   escape. *Nat. Rev. Microbiol.* 19:409–424.

711   Harvey WT, Carabelli AM, Jackson B, Gupta RK, Thomson EC, Harrison EM, Ludden C, Reeve R, Rambaut
712   A, COVID-19 Genomics UK (COG-UK) Consortium, et al. 2021. SARS-CoV-2 variants, spike
713   mutations and immune escape. *Nat. Rev. Microbiol.* 19:409–424.

714   Henderson R, Edwards RJ, Mansouri K, Janowska K, Stalls V, Gobeil SMC, Kopp M, Li D, Parks R, Hsu AL,
715   et al. 2020. Controlling the SARS-CoV-2 spike glycoprotein conformation. *Nat. Struct. Mol. Biol.*
716   27:925–933.

717   Hoffmann M, Kleine-Weber H, Schroeder S, Krüger N, Herrler T, Erichsen S, Schiergens TS, Herrler G, Wu
718   N-H, Nitsche A, et al. 2020. SARS-CoV-2 Cell Entry Depends on ACE2 and TMPRSS2 and Is
719   Blocked by a Clinically Proven Protease Inhibitor. *Cell* 181:271-280.e8.

720   Hong Q, Han W, Li J, Xu S, Wang Yifan, Xu C, Li Z, Wang Yanxing, Zhang C, Huang Z, et al. 2022. Molecular
721   basis of receptor binding and antibody neutralization of Omicron. *Nature* 604:546–552.

722   Houhamdi L, Gautret P, Hoang VT, Fournier P, Colson P, Raoult D. 2022. Characteristics of the first 1119
723   SARS-CoV-2 Omicron variant cases, in Marseille, France, November–December 2021. *J. Med.*
724   *Virol.* 94:2290–2295.

725   Huang Y, Yang C, Xu X, Xu W, Liu S. 2020. Structural and functional properties of SARS-CoV-2 spike
726   protein: potential antivirus drug development for COVID-19. *Acta Pharmacol. Sin.* 41:1141–
727   1149.

728   Hünenberger PH. 2005. Thermostat Algorithms for Molecular Dynamics Simulations. In: Dr. Holm C, Prof.
729   Dr. Kremer K, editors. Advanced Computer Simulation. Vol. 173. Berlin, Heidelberg: Springer
730   Berlin Heidelberg. p. 105–149. Available from: http://link.springer.com/10.1007/b99427

731   Jackson CB, Farzan M, Chen B, Choe H. 2022. Mechanisms of SARS-CoV-2 entry into cells. *Nat. Rev. Mol.*
732   *Cell Biol.* 23:3–20.

733   Kazan IC, Mills JH, Ozkan SB. 2023. Allosteric regulatory control in dihydrofolate reductase is revealed by
734   dynamic asymmetry. *Protein Sci.* 32:e4700.

735   Kazan IC, Sharma P, Rahman MI, Bobkov A, Fromme R, Ghirlanda G, Ozkan SB. 2022. Design of novel
736   cyanovirin-N variants by modulation of binding dynamics through distal mutations. *eLife*
737   11:e67474.

738   Kemp SA, Collier DA, Datir RP, Ferreira IATM, Gayed S, Jahun A, Hosmillo M, Rees-Spear C, Mlcochova P,
739   Lumb IU, et al. 2021. SARS-CoV-2 evolution during treatment of chronic infection. *Nature*
740   592:277–282.

741   Keskin O, Bahar I, Jernigan RL, Beutler JA, Shoemaker RH, Sausville EA, Covell DG. 2000. Characterization
742   of anticancer agents by their growth inhibitory activity and relationships to mechanism of action
743   and structure. *Anticancer. Drug Des.* 15:79–98.

744   Khan A, Zia T, Suleman M, Khan T, Ali SS, Abbasi AA, Mohammad A, Wei D. 2021. Higher infectivity of the
745   SARS-CoV-2 new variants is associated with K417N/T, E484K, and N501Y mutants: An insight
746   from structural data. *J. Cell. Physiol.* 236:7045–7057.

747   Kim, H., Zou, T., Modi, C., Dörner, K., Grunkemeyer, T.J., Chen, L., Fromme, R., Matz, M. V., Ozkan, S.B.,
748   Wachter, R.M. 2015. A hinge migration mechanism unlocks the evolution of green-to-red
749   photoconversion in GFP-like proteins. *Structure* 23:34–43.

750   Kim Sinae, Nguyen TT, Taitt AS, Jhun H, Park H-Y, Kim S-H, Kim Y-G, Song EY, Lee Y, Yum H, et al. 2021.
751   SARS-CoV-2 Omicron Mutation Is Faster than the Chase: Multiple Mutations on Spike/ACE2
752   Interaction Residues. *Immune Netw.* 21:e38.

753   Kimura, Motoo. 1983. The neutral theory of molecular evolution. Cambridge University Press

754   Kirchdoerfer RN, Cottrell CA, Wang N, Pallesen J, Yassine HM, Turner HL, Corbett KS, Graham BS,
755   McLellan JS, Ward AB. 2016. Pre-fusion structure of a human coronavirus spike protein. *Nature*
756   531:118–121.

757   Kistler KE, Huddleston J, Bedford T. 2022. Rapid and parallel adaptive mutations in spike S1 drive clade
758   success in SARS-CoV-2. *Cell Host Microbe* 30:545-555.e4.

759   Klinakis A, Cournia Z, Rampias T. 2021. N-terminal domain mutations of the spike protein are structurally
760   implicated in epitope recognition in emerging SARS-CoV-2 strains. *Comput. Struct. Biotechnol. J.*
761   19:5556–5567.

762   Kolbaba-Kartchner B, Kazan IC, Mills JH, Ozkan SB. 2021. The Role of Rigid Residues in Modulating TEM-1
763   β-Lactamase Function and Thermostability. *Int. J. Mol. Sci.* 22:2895.

764   Kumar, A., Glembo, T.J., Ozkan, S.B. 2015b. The Role of Conformational Dynamics and Allostery in the
765   Disease Development of Human Ferritin. *Biophys J* 109:1273–1281.

766   Kumar S, Stecher G, Li M, Knyaz C, Tamura K. 2018. MEGA X: Molecular Evolutionary Genetics Analysis
767   across Computing Platforms.Battistuzzi FU, editor. *Mol. Biol. Evol.* 35:1547–1549.

768   Kumar S, Tao Q, Weaver S, Sanderford M, Caraballo-Ortiz MA, Sharma S, Pond SLK, Miura S. 2021. An
769   Evolutionary Portrait of the Progenitor SARS-CoV-2 and Its Dominant Offshoots in COVID-19
770   Pandemic.Yeager M, editor. *Mol. Biol. Evol.* 38:3046–3059.

771   Kuzmanic A, Bowman GR, Juarez-Jimenez J, Michel J, Gervasio FL. 2020. Investigating Cryptic Binding
772   Sites by Molecular Dynamics Simulations. *Acc. Chem. Res.* 53:654–661.

773   Labbadia J, Morimoto RI. 2015. The Biology of Proteostasis in Aging and Disease. *Annu. Rev. Biochem.*
774   84:435–464.

775   Laiton-Donato K, Franco-Muñoz C, Álvarez-Díaz DA, Ruiz-Moreno HA, Usme-Ciro JA, Prada DA, Reales-
776   González J, Corchuelo S, Herrera-Sepúlveda MT, Naizaque J, et al. 2021. Characterization of the
777   emerging B.1.621 variant of interest of SARS-CoV-2. *Infect. Genet. Evol.* 95:105038.

778   Lan J, Ge J, Yu J, Shan S, Zhou H, Fan S, Zhang Q, Shi X, Wang Q, Zhang L, et al. 2020. Structure of the
779   SARS-CoV-2 spike receptor-binding domain bound to the ACE2 receptor. *Nature* 581:215–220.

780   Larrimore KE, Kazan IC, Kannan L, Kendle RP, Jamal T, Barcus M, Bolia A, Brimijoin S, Zhan C-G, Ozkan SB,
781   et al. 2017. Plant-expressed cocaine hydrolase variants of butyrylcholinesterase exhibit altered
782   allosteric effects of cholinesterase activity and increased inhibitor sensitivity. *Sci. Rep.* 7:10419.

783   Levy RM, Haldane A, Flynn WF. 2017. Potts Hamiltonian models of protein co-variation, free energy
784   landscapes, and evolutionary fitness. *Curr. Opin. Struct. Biol.* 43:55–62.

785   Liu L, Tamura K, Sanderford M, Gray VE, Kumar S. 2016. A Molecular Evolutionary Reference for the
786   Human Variome. *Mol. Biol. Evol.* 33:245–254.

787   Liu Xueyan, Liu Xuan, Zhou J, Dong Y, Jiang Wen, Jiang Wenqing. 2022. Rampant C-to-U deamination
788   accounts for the intrinsically high mutation rate in SARS-CoV-2 spike gene. *RNA* 28:917–926.

789   Liu Y, Bahar I. 2012. Sequence Evolution Correlates with Structural Dynamics. *Mol. Biol. Evol.* 29:2253–
790   2263.

791   Ma B, Nussinov R. 2016. Conformational footprints. *Nat. Chem. Biol.* 12:890–891.

792   Maguid S, Fernandez-Alberti S, Echave J. 2008. Evolutionary conservation of protein vibrational
793   dynamics. *Gene* 422:7–13.

794   Maguid S, Fernández-Alberti S, Parisi G, Echave J. 2006. Evolutionary Conservation of Protein Backbone
795   Flexibility. *J. Mol. Evol.* 63:448–457.

796   Maher MC, Bartha I, Weaver S, Di Iulio J, Ferri E, Soriaga L, Lempp FA, Hie BL, Bryson B, Berger B, et al.
797   2022. Predicting the mutational drivers of future SARS-CoV-2 variants of concern. *Sci. Transl.*
798   *Med.* 14:eabk3445.

799   Maier JA, Martinez C, Kasavajhala K, Wickstrom L, Hauser KE, Simmerling C. 2015. ff14SB: Improving the
800   Accuracy of Protein Side Chain and Backbone Parameters from ff99SB. *J. Chem. Theory Comput.*
801   11:3696–3713.

802   Markov PV, Ghafari M, Beer M, Lythgoe K, Simmonds P, Stilianakis NI, Katzourakis A. 2023. The evolution
803   of SARS-CoV-2. *Nat. Rev. Microbiol.* 21:361–379.

804   Menni C, Valdes AM, Polidori L, Antonelli M, Penamakuri S, Nogal A, Louca P, May A, Figueiredo JC, Hu C,
805   et al. 2022. Symptom prevalence, duration, and risk of hospital admission in individuals infected
806   with SARS-CoV-2 during periods of omicron and delta variant dominance: a prospective
807   observational study from the ZOE COVID Study. *The Lancet* 399:1618–1624.

808   Mikulska-Ruminska K, Shrivastava I, Krieger J, Zhang S, Li H, Bayır H, Wenzel SE, VanDemark AP, Kagan
809   VE, Bahar I. 2019. Characterization of Differential Dynamics, Specificity, and Allostery of
810   Lipoxygenase Family Members. *J. Chem. Inf. Model.* 59:2496–2508.

811   Millet JK, Whittaker GR. 2014. Host cell entry of Middle East respiratory syndrome coronavirus after
812   two-step, furin-mediated activation of the spike protein. *Proc. Natl. Acad. Sci.* 111:15214–
813   15219.

814   Millet JK, Whittaker GR. 2015. Host cell proteases: Critical determinants of coronavirus tropism and
815   pathogenesis. *Virus Res.* 202:120–134.

816   Mishra SK, Jernigan RL. 2018. Protein dynamic communities from elastic network models align closely to
817   the communities defined by molecular dynamics.Zhang Y, editor. *PLOS ONE* 13:e0199225.

818   Modi T, Campitelli P, Kazan IC, Ozkan SB. 2021. Protein folding stability and binding interactions through
819   the lens of evolution: a dynamical perspective. *Curr. Opin. Struct. Biol.* 66:207–215.

820   Modi T, Ozkan S. 2018. Mutations Utilize Dynamic Allostery to Confer Resistance in TEM-1 β-lactamase.
821   *Int. J. Mol. Sci.* 19:3808.

822   Modi T, Risso VA, Martinez-Rodriguez S, Gavira JA, Mebrat MD, Van Horn WD, Sanchez-Ruiz JM, Banu
823   Ozkan S. 2021. Hinge-shift mechanism as a protein design principle for the evolution of β-
824   lactamases from substrate promiscuity to specificity. *Nat. Commun.* 12:1852.

825   Moulana A, Dupic T, Phillips AM, Chang J, Nieves S, Roffler AA, Greaney AJ, Starr TN, Bloom JD, Desai
826   MM. 2022a. Compensatory epistasis maintains ACE2 affinity in SARS-CoV-2 Omicron BA.1. *Nat.*
827   *Commun.* 13:7011.

828   Moulana A, Dupic T, Phillips AM, Chang J, Nieves S, Roffler AA, Greaney AJ, Starr TN, Bloom JD, Desai
829   MM. 2022b. Compensatory epistasis maintains ACE2 affinity in SARS-CoV-2 Omicron BA.1. *Nat.*
830   *Commun.* 13:7011.

831   Moulana A, Dupic T, Phillips AM, Chang J, Roffler AA, Greaney AJ, Starr TN, Bloom JD, Desai MM. 2023.
832   The landscape of antibody binding affinity in SARS-CoV-2 Omicron BA.1 evolution. *eLife*
833   12:e83442.

834   Neher RA. 2022. Contributions of adaptation and purifying selection to SARS-CoV-2 evolution. *Virus Evol.*
835   8:veac113.

836   Nevin Gerek, Z., Kumar, S., Banu Ozkan, S. 2013. Structural dynamics flexibility informs function and
837   evolution at a proteome scale. *Evol Appl*.

838   Nielsen BF, Li Y, Sneppen K, Simonsen L, Viboud C, Levin SA, Grenfell BT. 2022. Immune Heterogeneity
839   and Epistasis Explain Punctuated Evolution of SARS-CoV-2. Epidemiology Available from:
840   http://medrxiv.org/lookup/doi/10.1101/2022.07.27.22278129

841   Nussinov, R., Tsai, C.-J. 2013. Allostery in disease and in drug discovery. *Cell* 153:293–305.

842   O'Rourke KF, Gorman SD, Boehr DD. 2016. Biophysical and computational methods to analyze amino
843   acid interaction networks in proteins. *Comput. Struct. Biotechnol. J.* 14:245–251.

844   Ose NJ, Butler BM, Kumar A, Kazan IC, Sanderford M, Kumar S, Ozkan SB. 2022. Dynamic coupling of
845   residues within proteins as a mechanistic foundation of many enigmatic pathogenic missense
846   variants.Wallqvist A, editor. *PLOS Comput. Biol.* 18:e1010006.

847   Ose NJ, Campitelli P, Patel RP, Ozkan SB, Kumar S. 2022. Protein dynamics provide mechanistic insights
848   about the epistatic relationships among highly observed potentially adaptive missense variants.
849   *Biophys. J.* 121:456a.

850   Otten R, Liu L, Kenner LR, Clarkson MW, Mavor D, Tawfik DS, Kern D, Fraser JS. 2018. Rescue of
851   conformational dynamics in enzyme catalysis by directed evolution. *Nat. Commun.* 9:1314.

852   Ozono S, Zhang Y, Ode H, Sano K, Tan TS, Imai K, Miyoshi K, Kishigami S, Ueno T, Iwatani Y, et al. 2021.
853   SARS-CoV-2 D614G spike mutation increases entry efficiency with enhanced ACE2-binding
854   affinity. *Nat. Commun.* 12:848.

855   Patel R, Scheinfeldt LB, Sanderford MD, Lanham TR, Tamura K, Platt A, Glicksberg BS, Xu K, Dudley JT,
856   Kumar S. 2018. Adaptive Landscape of Protein Variation in Human Exomes.Yeager M, editor.
857   *Mol. Biol. Evol.* 35:2015–2025.

858   de la Paz JA, Nartey CM, Yuvaraj M, Morcos F. 2020. Epistatic contributions promote the unification of
859   incompatible models of neutral molecular evolution. *Proc. Natl. Acad. Sci.* 117:5873–5882.

860   Pearlman DA, Case DA, Caldwell JW, Ross WS, Cheatham III TE, DeBolt S, Ferguson D, Seibel G, Kollman
861   P. 1995. AMBER, a package of computer programs for applying molecular mechanics, normal
862   mode analysis, molecular dynamics and free energy calculations to simulate the structural and
863   energetic properties of molecules. *Comput Phys Commun* 91:1–41.

864   Peters AD, Lively CM. 1999. The Red Queen and Fluctuating Epistasis: A Population Genetic Analysis of
865   Antagonistic Coevolution. *Am. Nat.* 154:393–405.

866   Qu P, Faraone JN, Evans JP, Zheng Y-M, Carlin C, Anghelina M, Stevens P, Fernandez S, Jones D, Panchal
867   A, et al. 2023. Extraordinary Evasion of Neutralizing Antibody Response by Omicron XBB.1.5,
868   CH.1.1 and CA.3.1 Variants. Microbiology Available from:
869   http://biorxiv.org/lookup/doi/10.1101/2023.01.16.524244

870   Raghuvamsi PV, Tulsian NK, Samsudin F, Qian X, Purushotorman K, Yue G, Kozma MM, Hwa WY, Lescar J,
871   Bond PJ, et al. 2021. SARS-CoV-2 S protein:ACE2 interaction reveals novel allosteric targets. *eLife*
872   10:e63646.

873   Ramarao-Milne P, Jain Y, Sng LMF, Hosking B, Lee C, Bayat A, Kuiper M, Wilson LOW, Twine NA, Bauer
874   DC. 2022. Data-driven platform for identifying variants of interest in COVID-19 virus. *Comput.*
875   *Struct. Biotechnol. J.* 20:2942–2950.

876   Rehman S ur, Shafique L, Ihsan A, Liu Q. 2020. Evolutionary Trajectory for the Emergence of Novel
877   Coronavirus SARS-CoV-2. *Pathogens* 9:240.

878   Rizzato F, Coucke A, de Leonardis E, Barton JP, Tubiana J, Monasson R, Cocco S. 2020. Inference of
879   compressed Potts graphical models. *Phys. Rev. E* 101:012309.

880   Rochman ND, Faure G, Wolf YI, Freddolino PL, Zhang F, Koonin EV. 2022. Epistasis at the SARS-CoV-2
881   Receptor-Binding Domain Interface and the Propitiously Boring Implications for Vaccine
882   Escape.Diamond MS, editor. *mBio* 13:e00135-22.

883   Rochman ND, Wolf YI, Faure G, Mutz P, Zhang F, Koonin EV. 2021. Ongoing global and regional adaptive
884   evolution of SARS-CoV-2. *Proc. Natl. Acad. Sci.* 118:e2104241118.

885   Rodriguez-Rivas J, Croce G, Muscat M, Weigt M. 2022. Epistatic models predict mutable sites in SARS-
886   CoV-2 proteins and epitopes. *Proc. Natl. Acad. Sci.* 119:e2113118119.

887   Rojas Echenique JI, Kryazhimskiy S, Nguyen Ba AN, Desai MM. 2019. Modular epistasis and the
888   compensatory evolution of gene deletion mutants.Butler G, editor. *PLOS Genet.* 15:e1007958.

889   Saavedra HG, Wrabl JO, Anderson JA, Li J, Hilser VJ. 2018. Dynamic allostery can drive cold adaptation in
890   enzymes. *Nature* 558:324–328.

891   Saputri DS, Li S, van Eerden FJ, Rozewicki J, Xu Z, Ismanto HS, Davila A, Teraguchi S, Katoh K, Standley
892   DM. 2020. Flexible, Functional, and Familiar: Characteristics of SARS-CoV-2 Spike Protein
893   Evolution. *Front. Microbiol.* 11:2112.

894   Sekhar A, Kay LE. 2019. An NMR View of Protein Dynamics in Health and Disease. *Annu. Rev. Biophys.*
895   48:297–319.

896   Shang J, Wan Y, Luo C, Ye G, Geng Q, Auerbach A, Li F. 2020. Cell entry mechanisms of SARS-CoV-2. *Proc.*
897   *Natl. Acad. Sci.* 117:11727–11734.

898   Shimagaki K, Weigt M. 2019. Selection of sequence motifs and generative Hopfield-Potts models for
899   protein families. *Phys. Rev. E* 100:032128.

900   Shoemark DK, Oliveira ASF, Davidson AD, Berger I, Schaffitzel C, Mulholland AJ. 2022. Molecular
901   dynamics of spike variants in the locked conformation: RBD interfaces, fatty acid binding and
902   furin cleavage sites. Biochemistry Available from:
903   http://biorxiv.org/lookup/doi/10.1101/2022.05.06.490927

904   Singh D, Yi SV. 2021. On the origin and evolution of SARS-CoV-2. *Exp. Mol. Med.* 53:537–547.

905   Spinello A, Saltalamacchia A, Borišek J, Magistrato A. 2021. Allosteric Cross-Talk among Spike's Receptor-
906   Binding Domain Mutations of the SARS-CoV-2 South African Variant Triggers an Effective
907   Hijacking of Human Cell Receptor. *J. Phys. Chem. Lett.* 12:5987–5993.

908   Starr TN, Greaney AJ, Hannon WW, Loes AN, Hauser K, Dillen JR, Ferri E, Farrell AG, Dadonaite B,
909   McCallum M, et al. 2022. Shifting mutational constraints in the SARS-CoV-2 receptor-binding
910   domain during viral evolution. *Science* 377:420–424.

911   Starr TN, Greaney AJ, Stewart CM, Walls AC, Hannon WW, Veesler D, Bloom JD. 2022. Deep mutational
912   scans for ACE2 binding, RBD expression, and antibody escape in the SARS-CoV-2 Omicron BA.1
913   and BA.2 receptor-binding domains.Mok CKP, editor. *PLOS Pathog.* 18:e1010951.

914   Starr TN, Zepeda SK, Walls AC, Greaney AJ, Alkhovsky S, Veesler D, Bloom JD. 2022. ACE2 binding is an
915   ancestral and evolvable trait of sarbecoviruses. *Nature* 603:913–918.

916   Steinhauer DA. 1999. Role of Hemagglutinin Cleavage for the Pathogenicity of Influenza Virus. *Virology*
917   258:1–20.

918   Stevens AO, Kazan IC, Ozkan B, He Y. 2022. Investigating the allosteric response of the PICK1 PDZ domain
919   to different ligands with all-atom simulations. *Protein Sci.* 31:e4474.

920   Sun PA Y, Kollman. 1995. Hydrophobic solvation of methane and nonbond parameters of the TIP3P
921   water model. *J Comput Chem* 16:1164–1169.

922   Swint-Kruse L, Matthews KS, Smith PE, Pettitt BM. 1998. Comparison of Simulated and Experimentally
923   Determined Dynamics for a Variant of the LacI DNA-Binding Domain, Nlac-P. *Biophys. J.* 74:413–
924   421.

925   Sztain T, Ahn S-H, Bogetti AT, Casalino L, Goldsmith JA, Seitz E, McCool RS, Kearns FL, Acosta-Reyes F,
926   Maji S, et al. 2021. A glycan gate controls opening of the SARS-CoV-2 spike protein. *Nat. Chem.*
927   13:963–968.

928   Tan ZW, Tee W-V, Samsudin F, Guarnera E, Bond PJ, Berezovsky IN. 2022. Allosteric perspective on the
929   mutability and druggability of the SARS-CoV-2 Spike protein. *Structure* 30:590-607.e4.

930   Tang X, Wu C, Li X, Song Y, Yao X, Wu X, Duan Y, Zhang H, Wang Y, Qian Z, et al. 2020. On the origin and
931   continuing evolution of SARS-CoV-2. *Natl. Sci. Rev.* 7:1012–1023.

932   Tay JH, Porter AF, Wirth W, Duchene S. 2022. The Emergence of SARS-CoV-2 Variants of Concern Is
933   Driven by Acceleration of the Substitution Rate.Leitner T, editor. *Mol. Biol. Evol.* 39:msac013.

934   Teruel N, Mailhot O, Najmanovich RJ. 2021. Modelling conformational state dynamics and its role on
935   infection for SARS-CoV-2 Spike protein variants.Dunbrack RL, editor. *PLOS Comput. Biol.*
936   17:e1009286.

937   Thye AY-K, Law JW-F, Pusparajah P, Letchumanan V, Chan K-G, Lee L-H. 2021. Emerging SARS-CoV-2
938   Variants of Concern (VOCs): An Impending Global Crisis. *Biomedicines* 9:1303.

939   Walls AC, Park Y-J, Tortorici MA, Wall A, McGuire AT, Veesler D. 2020. Structure, Function, and
940   Antigenicity of the SARS-CoV-2 Spike Glycoprotein. *Cell* 181:281-292.e6.

941   Wang Q, Guo Y, Iketani S, Nair MS, Li Z, Mohri H, Wang M, Yu J, Bowen AD, Chang JY, et al. 2022.
942   Antibody evasion by SARS-CoV-2 Omicron subvariants BA.2.12.1, BA.4 and BA.5. *Nature*
943   608:603–608.

944   Wang Q, Iketani S, Li Z, Liu Liyuan, Guo Y, Huang Y, Bowen AD, Liu M, Wang M, Yu J, et al. 2022. Alarming
945   antibody evasion properties of rising SARS-CoV-2 BQ and XBB subvariants.
946   *Cell*:S0092867422015318.

947   Weisblum Y, Schmidt F, Zhang F, DaSilva J, Poston D, Lorenzi JC, Muecksch F, Rutkowska M, Hoffmann H-
948   H, Michailidis E, et al. 2020. Escape from neutralizing antibodies by SARS-CoV-2 spike protein
949   variants. *eLife* 9:e61312.

950   Witte L, Baharani VA, Schmidt F, Wang Z, Cho A, Raspe R, Guzman-Cardozo C, Muecksch F, Canis M, Park
951   DJ, et al. 2023. Epistasis lowers the genetic barrier to SARS-CoV-2 neutralizing antibody escape.
952   *Nat. Commun.* 14:302.

953   Wrapp D, Wang N, Corbett KS, Goldsmith JA, Hsieh C-L, Abiona O, Graham BS, McLellan JS. 2020. Cryo-
954   EM structure of the 2019-nCoV spike in the prefusion conformation. *Science* 367:1260–1263.

955   Wrobel AG, Benton DJ, Xu P, Roustan C, Martin SR, Rosenthal PB, Skehel JJ, Gamblin SJ. 2020. SARS-CoV-
956   2 and bat RaTG13 spike glycoprotein structures inform on virus evolution and furin-cleavage
957   effects. *Nat. Struct. Mol. Biol.* 27:763–767.

958   Wu L, Zhou L, Mo M, Liu T, Wu C, Gong C, Lu K, Gong L, Zhu W, Xu Z. 2022. SARS-CoV-2 Omicron RBD
959   shows weaker binding affinity than the currently dominant Delta variant to human ACE2. *Signal*
960   *Transduct. Target. Ther.* 7:8.

961   Xue Q, Liu X, Pan W, Zhang A, Fu J, Jiang G. 2022. Computational Insights into the Allosteric Effect and
962   Dynamic Structural Features of the SARS-COV-2 Spike Protein. *Chem. – Eur. J.* [Internet] 28.
963   Available from: https://onlinelibrary.wiley.com/doi/10.1002/chem.202104215

964   Yang QE, MacLean C, Papkou A, Pritchard M, Powell L, Thomas D, Andrey DO, Li M, Spiller B, Yang W, et
965   al. 2020. Compensatory mutations modulate the competitiveness and dynamics of plasmid-
966   mediated colistin resistance in Escherichia coli clones. *ISME J.* 14:861–865.

967   Yue C, Song W, Wang L, Jian F, Chen X, Gao F, Shen Z, Wang Y, Wang X, Cao Y. 2023. Enhanced
968   transmissibility of XBB.1.5 is contributed by both strong ACE2 binding and antibody evasion.
969   Immunology Available from: http://biorxiv.org/lookup/doi/10.1101/2023.01.03.522427

970   Yurkovetskiy L, Wang X, Pascal KE, Tomkins-Tinch C, Nyalile TP, Wang Y, Baum A, Diehl WE, Dauphin A,
971   Carbone C, et al. 2020. Structural and Functional Analysis of the D614G SARS-CoV-2 Spike
972   Protein Variant. *Cell* 183:739-751.e8.

973   Zeng H-L, Dichio V, Rodríguez Horta E, Thorell K, Aurell E. 2020. Global analysis of more than 50,000
974   SARS-CoV-2 genomes reveals epistasis between eight viral genes. *Proc. Natl. Acad. Sci.*
975   117:31519–31526.

976   Zhang J, Cai Y, Xiao T, Lu J, Peng H, Sterling SM, Walsh RM, Rits-Volloch S, Zhu H, Woosley AN, et al.
977   2021. Structural impact on SARS-CoV-2 spike protein by D614G substitution. *Science* 372:525–
978   530.

979   Zhou T, Tsybovsky Y, Gorman J, Rapp M, Cerutti G, Chuang G-Y, Katsamba PS, Sampson JM, Schön A,
980   Bimela J, et al. 2020. Cryo-EM Structures of SARS-CoV-2 Spike without and with ACE2 Reveal a
981   pH-Dependent Switch to Mediate Endosomal Positioning of Receptor-Binding Domains. *Cell Host*
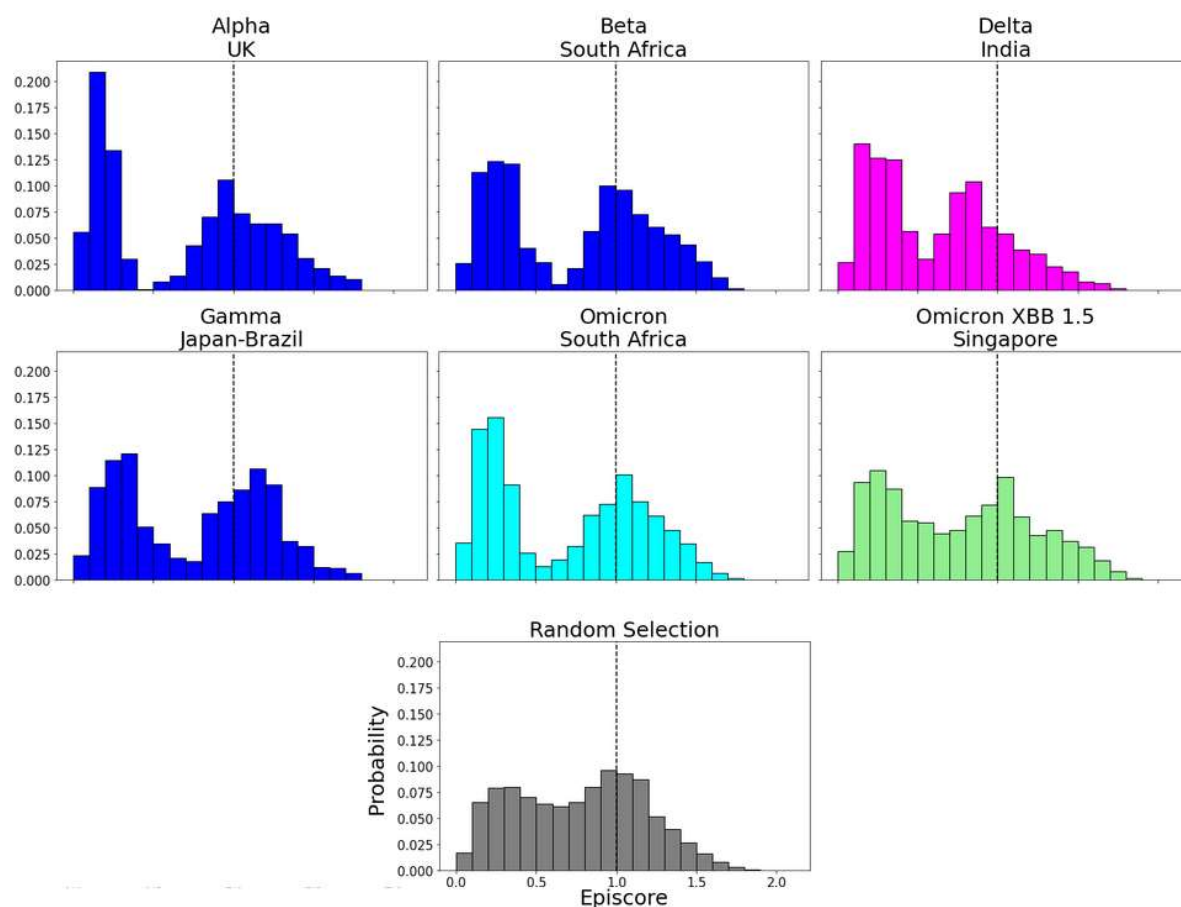982   *Microbe* 28:867-879.e5.

983
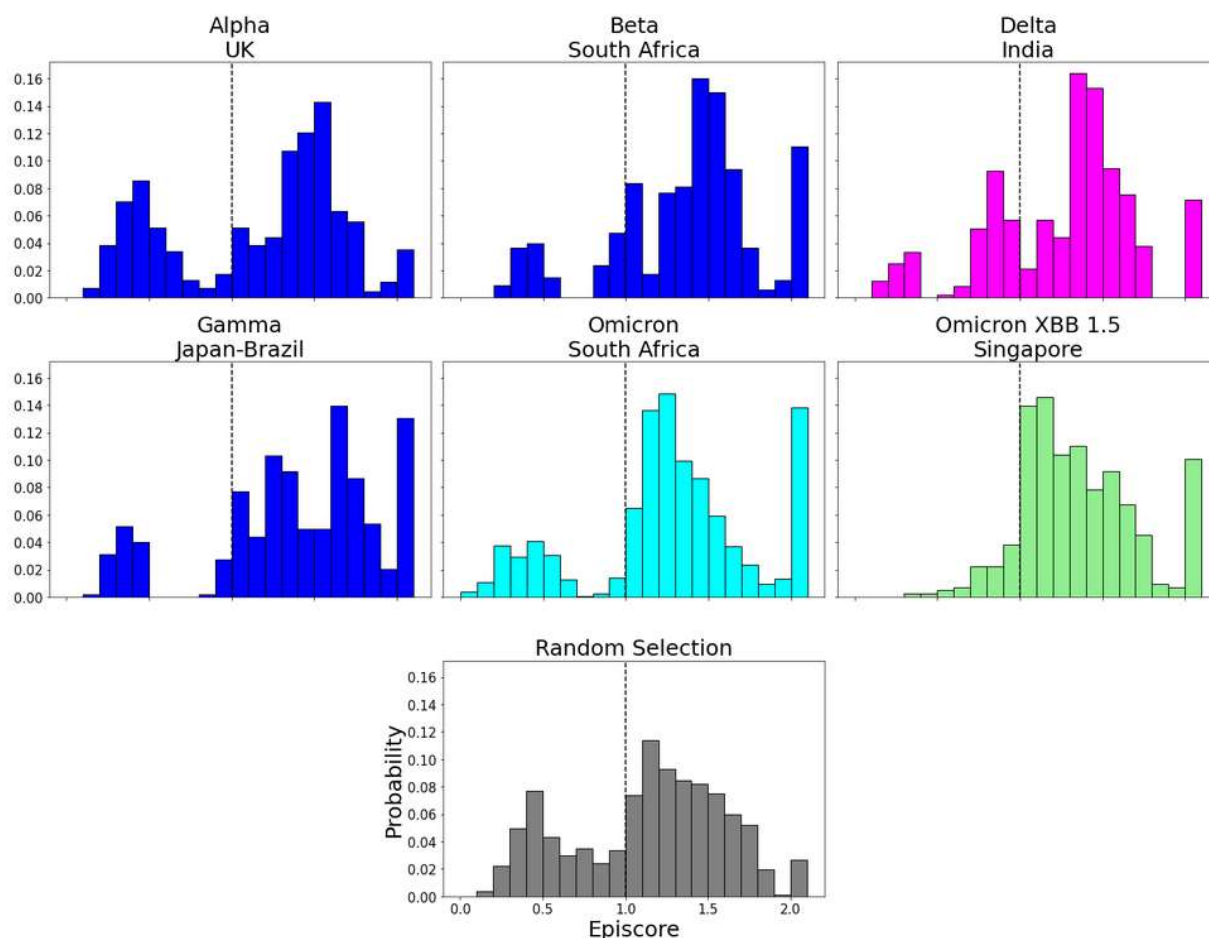
984

985   **Supplemental Figures**

986

987
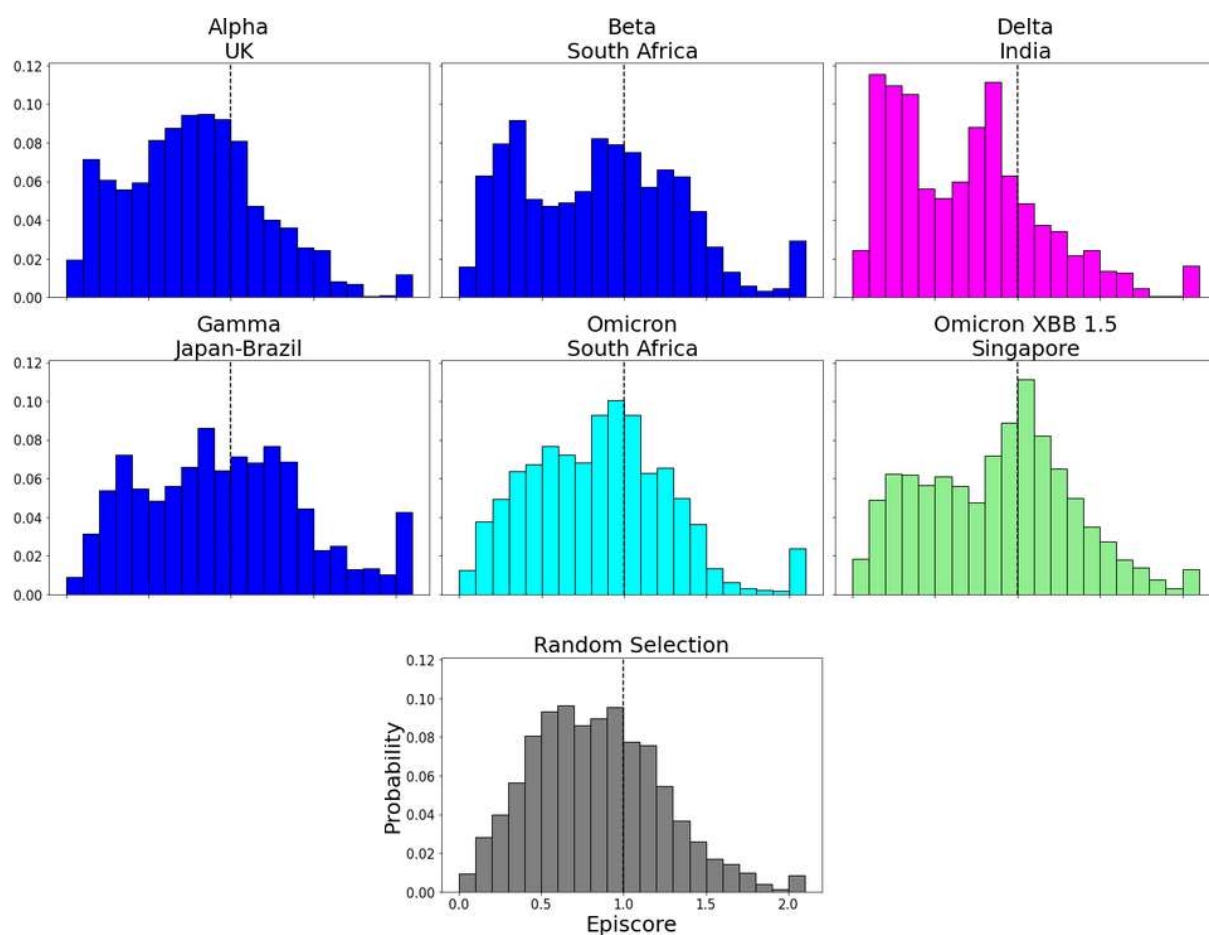
988   Supplementary figure S1. EpiScores with i = characteristic mutation sites, j = low EP sites, and k =

989   the binding interface of the open chain. EpiScores using variant sites are significantly different

990   (p<.001) from a set of EpiScores using random sites.

991

992

993 Supplementary figure S2. EpiScores with i = characteristic mutation sites within the NTD, j = low

994 EP sites, and k = the binding interface of the open chain. NTD domain mutation sites result in

995 markedly lower EpiScores compared to elsewhere.

996

997

998

999

1000   Supplementary figure S3. EpiScores with i = characteristic mutation sites, j = site 486, and k = the

1001   binding interface of the open chain. CAP and hACE2 and antibody binding site 486 displays

1002   epistasis with almost all XBB 1.5 variant sites at almost every hACE2 binding site. EpiScores

1003   using variant sites are significantly different (p<.001) from a set of EpiScores using random sites.

1004

1005